EVALUATION OF CLIMATE RISKS IN CHAO PHRAYA BASIN

Piotr Wolski[1],

Mark Tadross, Supattana Wichakul

[1] Climate System Analysis Group, University of Cape Town, South Africa

12 May 2021

EXECUTIVE SUMMARY

This report analyses historical observations and a suite of climate projections to evaluate future climate risks in the Chao Phraya basin and to ascertain the evidence for increasing risks of both floods, crop and irrigation water requirements.

Historical (post-1950s) climate trends are evaluated using a range of datasets – observational and gridded. Trends are weak and inconsistent and should not be interpreted as systematic drivers behind historical extreme events (such as the 2011 flood), nor as expressions of anthropogenic climate change.

Trends in air temperature are, however, relatively strong and consistent, with consequent implications for evaporation and drought. There is no clear signal in rainfall-based drought indices, a rainfall-evaporation based index (SPEI) shows clear and consistent signals, with the overall increase in drought, and statistically significant increases in the frequency of SPEI-indexed drought during the last 100 years. These trends are consistent with global temperature trends and trends in GHG concentrations, and as such, are expected to increasingly affect local climates in the future.

Climate projections, utilizing multi-model, multi-method and multi-generational ensembles, indicate increases in rainfall in the long-term (particularly the latter part of the rainfall season during August to October), with signals emerging in the near future, and strong and consistent increases in air temperature, irrespective of the considered scenario of GHG emissions. Annually, projected changes rainfall and air temperature to a certain extent compensate for each other. This has implications for drought, with one consequence that future drought risk on annual and longer timescales is expected to increase in near term, but reduce in the long-term.

A strong impact is demonstrated of the projected increase in air temperature and PET on agricultural water demand in the near future: both crop water demand and irrigation water requirements increase by up to 30% compared to those in historical period. This shows that more irrigation water and improvements in the efficiency of its application will be needed to deal with the impact of climate change.

That projected increases in annual rainfall totals largely stem from a relatively strong increase in rainfall in the peak of the rainy season (Aug-Oct) explains why water discharges and floods are expected to increase, even though agricultural drought is also expected to increase. An earlier study (Wichakul et al. 2014) of the hydrological impacts of climate change clearly demonstrated that even weak rainfall increases are strongly amplified in the hydrological system to create a considerable impact on streamflow in the lower parts of the basin. Our results show that the rainfall estimates used in this previous study are from a model that lies close to the lower bound of the ensemble range and that it is therefore more likely that a wetter future will result in higher increases in water discharges and flood risk in the basin.

1 INTRODUCTION

1.1 OBJECTIVES:

To evaluate historical data and climate change projections for the Chao Phraya basin from the perspective of future climate risks, in particular to ascertain the evidence for increasing risks of both floods and droughts.

1.2 APPROACH:

The study is based on a review of available literature and analyses of primary observational (available station data from TMD and CRU gridded datasets) and climate model projections (CMIP5, CMIP6 and CORDEX), organized in the following steps:

- Analyses of historical climate data, focusing on long term (centennial scale) and recent (60-70 years, since 1951) trends and patterns in time-aggregate (monthly/seasonal) rainfall, surface air temperatures, drought and extreme event indices (as defined and calculated using the Climdex software[1]). These analyses are based on primary station data from 17 meteorological stations provided by the Thai Meteorological Department (TMD), as well as on derived gridded datasets (CRU v4.04[2]) and satellite-based data products (e.g. CHIRPS[3]).

- Analyses of climate projections across three generations and types of climate projection models i.e. global models from the CMIP5 and CMIP6[4] archives, as well as regionally downscaled climate models from the CORDEX[5] repository for East Asia. The focus is on time-aggregate indices (monthly/seasonal) rainfall, temperature, drought and extreme event indices.

- The above analyses of climate changes are used to contextualise a study of hydrological impacts of climate change (Wichakul et al., 2014, based on a single downscaled global model) within the landscape of multi-model, multi method climate projections. This approach demonstrates the simulated hydrological responses of the Chao Phraya basin to a given climate change forcing (using the MRI-AGCM3.2s), compares the climate forcing from this model to the full range of simulated climate forcings in the CMIP5, CMIP6 and CORDEX ensembles, and discusses the likelihood of further changes in rainfall and temperatures leading to greater or lesser likelihoods of floods and droughts

[1] https://www.climdex.org/

[2] https://crudata.uea.ac.uk/cru/data/hrg/

[3] https://www.chc.ucsb.edu/data/chirps

[4] https://www.wcrp-climate.org/wgcm-cmip/wgcm-cmip6

[5] https://cordex.org/domains/region-7-east-asia/

1.3 Data and Methods

1.3.1 Observational data

We utilize a daily rainfall and air temperature dataset from 17 stations within the Chao Phraya basin provided by Thai Meteorological Department.

This observational dataset is supplemented by freely available global gridded data products. These provide uniform spatial coverage across the entire basin, and allow an extension of temporal coverage of data (limited, however, due to uncertainties associated with reconstruction of rainfall time series from a set of stations with changing numbers and quality). Three different products are used here: CRU TS v.4.04 (Harris et al. 2020), GPCC v.2018 (Schneider et al. 2018) and CHIRPS v.2 (Funk et al. 2014) (thereafter simply CRU, GPCC and CHIRPS).

CRU and GPCC datasets are interpolated from monthly station data to a regular 0.5° latitude/longitude grid. Both rainfall and temperature (minimum and maximum) variables are available from CRU over the period of 1901-2019. The GPCC v.2018 dataset provides only rainfall values spanning the period 1900-2016, but these were merged with the GPCC Monitoring v.6 product so that the merged dataset spans until Dec 2019. The CHIRPS dataset is a blended station-satellite product of 0.25° resolution, spanning the period of 1982 until present.

1.3.2 Climate projections data

In order to include plausible projections of future rainfall in the region, three ensembles of projections using two generations of climate change models were used:

- multi-model Global Climate Model (GCM) ensembles produced by the most recent generation of models contributing to the CMIP6 archive,
- multi-model GCM ensembles produced by the previous generation of models contributing to the CMIP5 archive
- multi-model ensemble of Regional Climate Models (RCMs) from the CORDEX East Asia. These RCMs are used to dynamically downscale projections from CMIP5 GCMs.

CMIP5 and CMIP6 global climate models are relatively coarse resolution models (~100-200km grid size), and by their nature are not expected to provide spatially detailed information for the sub-regions of the Chao Phraya basin. They do, however, provide a large ensemble of estimated climate changes for the basin as a whole, and therefore provide an indication of the expected range of uncertainty of climate changes across the basin. CORDEX models are higher resolution (0.44 deg or ~ 50km and 0.22 deg or ~25 km), and as a result they provide higher resolution estimates of changes for Chao Phraya sub basins, albeit for a more limited set of climate models and hence limited range of possible estimates. Data for both 0.44 deg and 0.25 deg ensemble are available for RCP 8.5 scenario, but data for only 0.44 deg ensemble are available for the RCP 4.5 scenario.

All three ensembles exhibit large ensemble spread in rainfall projections (i.e. projected changes in rainfall vary considerably from model to model within each ensemble). We compared projections from all ensembles in order to gain a better insight into the range of projections' uncertainty, and improved confidence in estimates of the overall direction (positive/negative) and magnitude of projected changes.

In addition, we analysed the primary climate projections data used to evaluate hydrological consequences of climate change in the Chao Phraya basin by Wichakul et al. 2014. That study used a single simulation of future climate from a high resolution (~20 km) global climate model MRI-AGCM3.2s.

We focused analyses on projections under two GHG scenarios - non-conservative or high GHG emission scenarios - RCP 8.5 for CMIP5, and SSP 585 for CMIP6, and moderate emission scenario RCP 4.5 for CMIP5 and SSP 245 for CMIP6 scenario. The MRI model was run under SRES A1B emission scenario, which corresponds to a high emission scenario in the near future and moderate emissions in the far future.

1.3.3 Statistics describing extreme events

The characterize drought two commonly used drought indices were used, viz. Standardised Precipitation Index (SPI) (McKee et al. 1993) and Standardised Precipitation Evapotranspiration Index (SPEI) (Vicente-Serrano et al. 2010).

The SPI is a drought index based on standardized rainfall anomalies that can be derived over a range of temporal scales - typically between 1 and 36 months. SPEI is similar, with the difference that it accounts for the role of evaporation as one of drivers of drought. We focused on time scales of 12 and 36 months (1 and 3 years) as these represent time scales most relevant from the point of view of the impact of drought on water resources in perennial rivers such as the Chao Phraya.

To calculate the evaporation component of SPEI, the Thornthwaite formula (Allen et al. 1991) was used to calculate potential evapotranspiration from air temperature data. It was noted that the Thornthwaite formulation of evaporation does not include humidity and wind components, however, given the lack of available humidity and wind data for large spatial extents across the region, the Thornthwaite formulation is more pragmatic to use. Both SPI and SPEI are calculated on monthly data.

Additionally, we calculate several standard Climdex extreme rainfall indices:

- r95p - total precipitation from events when rainfall > 95th percentile
- r99p - total precipitation from events when rainfall > 99th percentile
- rx1day - maximum 1 day rainfall
- rx3day - maximum consecutive 3 day rainfall
- rx5day - maximum consecutive 5 day rainfall
- cdd - maximum length of dry spell: maximum number of consecutive days with rainfall < 1mm
- cwd - maximum length of wet spell: maximum number of consecutive days with rainfall > 1mm

We also evaluate the following extreme temperature indices:

- tnn - Minimum value of daily minimum temperature
- txn - maximum value of maximum daily temperature

- txge35 - percentage of days when maximum temperature > 35 deg C

Calculation of these indices used the Rclimdex library within the R statistical software package.

1.3.4 Analyses of historical trends

We use two approaches to evaluate trends, their magnitude, direction and statistical significance.

For variables and indices at the annual time scale - we use non-parametric Theil-Sen trend (Sen, 1968) with block bootstrap-based evaluation of trend significance. This approach offers a most robust way of determination of trend that takes into account the influence of persistence (serial correlation) on trend significance. Significance of trends in extreme rainfall indices, which are calculated using the RClimdex package, is derived with the approach implemented in that package, i.e. through Mann-Kendall non-parametric trend significance test.

Mann-Kendal test is also used in analyses of trends in frequency of drought events.

1.3.5 Analyses of climate projections

To illustrate climate projections, we use the so-called plume plots. A plume plot presents the temporal trajectory (a time series) of a given variable (e.g. total annual rainfall), or actually it's anomaly with respect to a selected reference period, as simulated by an ensemble of models in historical simulations and for the future. The "plume" spans the range of model-simulated values for each time step, and as such represents uncertainty of projections arising due to model uncertainty. Plume plots are constructed separately for each variable, and separately for each GHG emission scenario. We, however, overplot plumes for various multi-model ensembles (in this case - CMIP5, CMIP6 and CORDEX). This allows for an easy evaluation of agreement between the various ensembles. In addition, we superimpose the actual, historical trajectory of the observed variable, or multiple observed variables if there are different observational data sources (as is the case here with rainfall, which is available from CRU and GPCC datasets).

We construct the plumes in the following way:

- Plume plots are constructed for total annual rainfall and mean annual temperature. We use area average values for each of the sub-catchments.
- For each individual (model or observational) time series of annual values anomalies are calculated wrt. 1987-2006 mean. We calculate absolute anomalies for temperature and relative anomalies (% of mean) for rainfall.
- 30-year rolling average is calculated on each individual time series.
- The above steps ensure that all series used in plume plots align at the value of 0 over the 1987-2006 period.
- The rolling average series of observational data are plotted directly
- For each of the model ensembles, 5th and 95th percentile of the ensemble values are calculated for each year. These values are used to bound the plume.

- Additionally, we overplot the median of the ensemble, again, calculated individually for each year.

2 General - climate and hydrology of Chao-Phraya basin

Upper Chao Phraya basin has four main sub-catchments (west to east): Ping, Wang, Yom and Nan (Fig. 1). Mean annual rainfall is in the range of 1000-1700 mm/year, and there is a weak West to East gradient (Fig. 2). Rainfall distribution is bi-modal, with two peaks: May and August-October. The second peak occurs later (Sep-Oct) in the South, and earlier (Jul-Aug) in the North. Dec-Jan is a dry season (Fig. 3). Higher rainfall in peak seasons is associated with higher intensity of rainfall events, and the low rainfall in mid-season (Jun-Jul) results from lower intensity of events; there is no reduction in the event numbers during that period (Fig. 3). The dry season is in general cooler than the wet season, although the highest temperatures (and thus likely the highest potential evaporation) occur at the beginning of the rainy season - in Mar-Apr.

The Chao-Phraya river is perennial, with low flow season spanning Dec to May, and monomodal seasonality, with a peak in Sep-Oct. There is, clearly, little response of the river to the first (May) rainfall peak (Fig. 4). Streamflow hydrograph at the outlet of the upper basin is a superposition of a large seasonal swell with a number of smaller peaks related to individual rainfall events. This, combined with the fact that the annual streamflow peak occurs towards the end of the bi-modal rainy season, implies that from the perspective of flood risk, both seasonal rainfall accumulation, and the magnitude of individual rainfall events have to be considered.

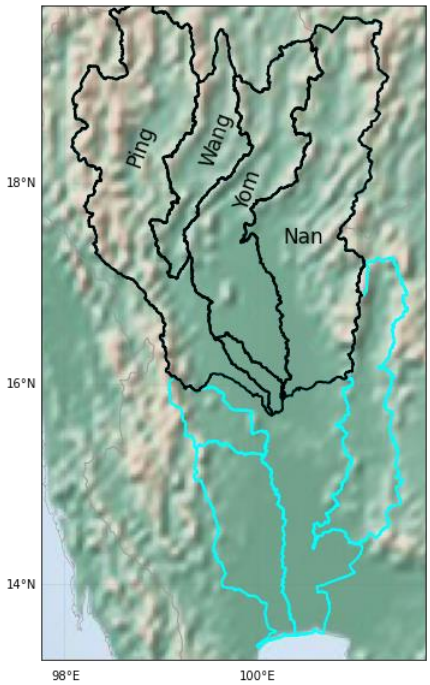

Figure 1: Subcatchments of the Chao Phraya basin

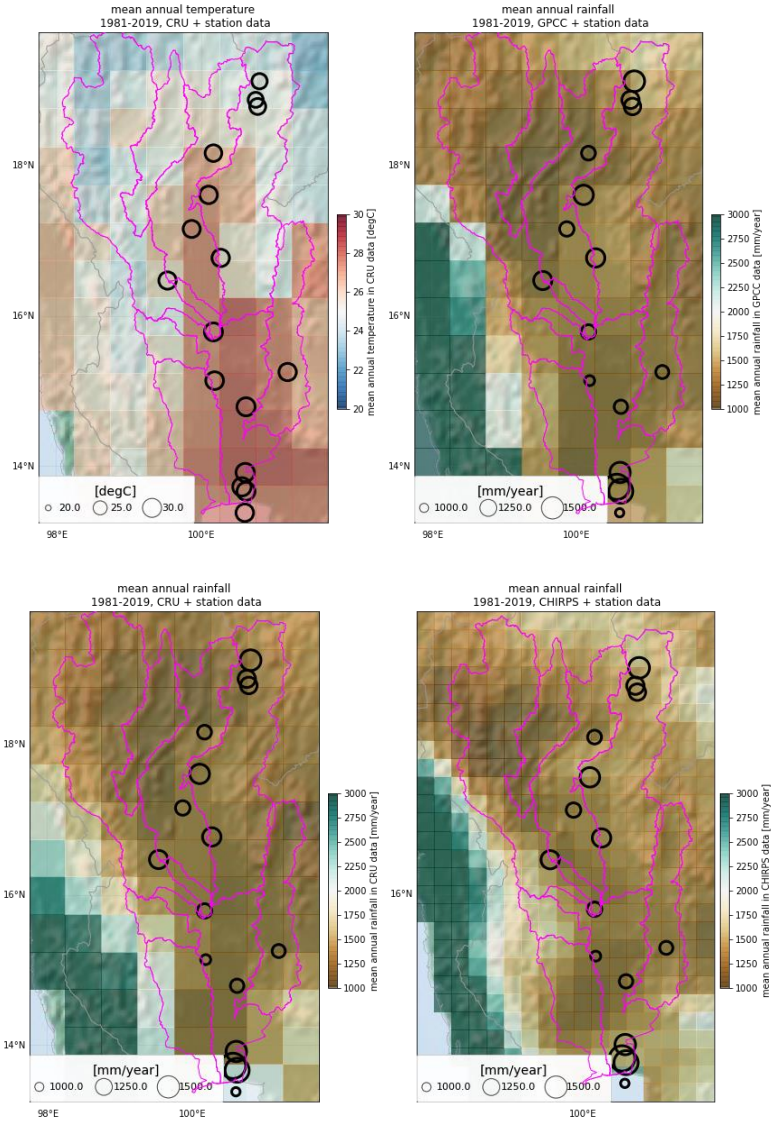

Figure 2: Spatial heterogeneity of rainfall and air temperature in the region - based on CHIRPS satellite rainfall dataset, GPCC and CRU gridded data and station data.

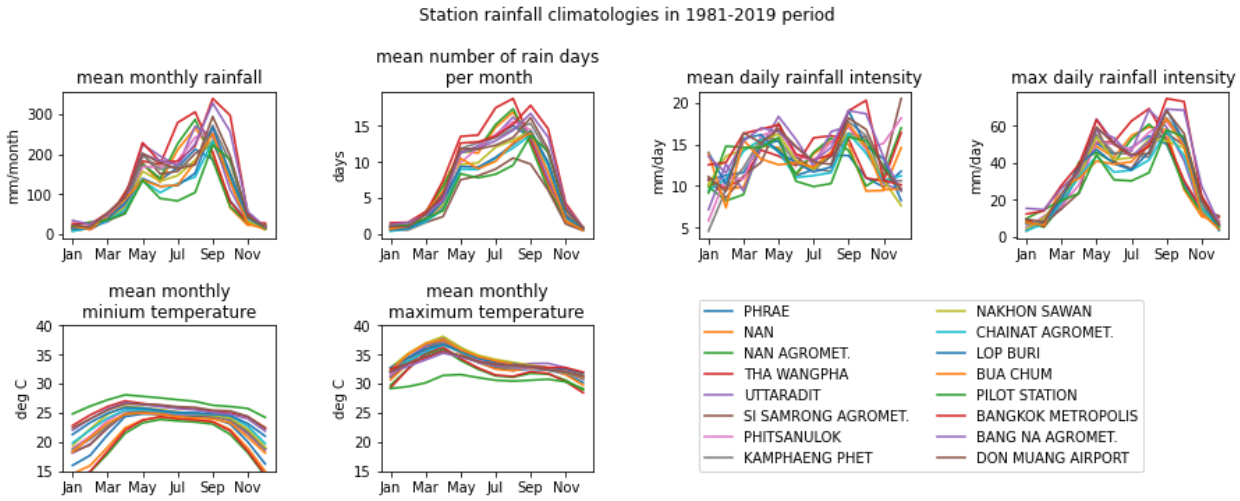

Figure 3: Seasonality of various rainfall and air temperature attributes based on station data

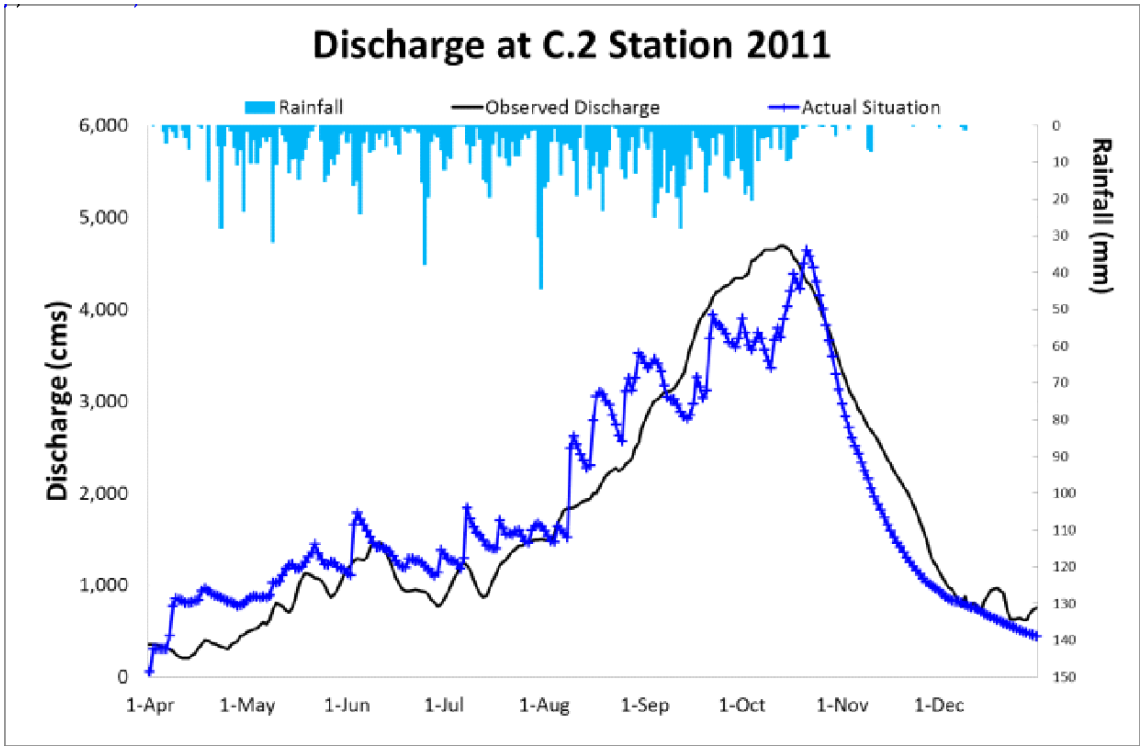

Figure 4: Discharge of Chao Phraya at the outlet of the upper basin. Figure from Wichakul et al. 2014.

3 HISTORICAL TRENDS

3.1 Approach

Due to the nature of flood events in the basin, which are a superposition of seasonal accumulation and individual events, we analyse trends in several attributes of rainfall.

Firstly, we evaluate trends station data in measures expressing the overall wetness, as well as the average intensity and frequency of rainfall events, namely: total rainfall, mean daily rainfall on a rainy day (>1mm) and number of rain days (>1mm), for the entire year (Fig. 5) and for the rainy season's peak (Aug-Oct - Fig. 6). In order to evaluate spatial heterogeneity of trends - we analyse trends in total annual rainfall in gridded CHIRPS data.

Subsequently, we evaluate trends in a number of extreme rainfall and temperature indices, listed in the Methods and Data section.

Finally, in order to capture trends in drought-relevant aspects of climate, we calculate trends in two drought indices: SPI and SPEI, calculated on 12 and 36-month time scales. These are calculated for each of the four sub-catchment using area-average of gridded rainfall and temperature from CRU data. We analyse trends in index value at the end of the calendar year (Dec), and also in the frequency of drought events defined by index value of less than -1 (moderate drought) at the end of calendar year.

3.2 Results

3.2.1 Mean rainfall and temperature

Overall, rainfall trends in the 1951-2019 period are weak although predominantly upward. The statistically significant increase is present only in stations near Bangkok (Fig. 5). The upward trends in total annual rainfall in Bangkok seem to be driven by an increase in the number of rain days rather than an increase in rainfall intensity.

Trends in rainfall characteristics of the main part of the rainy season (Aug-Oct) are diverse and weak. There seems to be no consistent trend in total season's rainfall, although some increase in rainfall intensity, compensated by a (mostly statisticaly significant) decrease in the number of rain days (Fig. 6). Trends in the Bangkok area appear to be somewhat different than in the rest of the analysed stations - there is an increase in the number of rain days compensated to a certain extent by the decrease in maximum rainfall intensity.

Trends in total annual rainfall in the gridded CHIRPS data correspond moderately well to those recorded at rainfall stations. In general, they indicate an increase in total annual rainfall across the entire basin. CHIRPS trends are only locally statistically significant, mostly in the upper section of the basin, which is in contrast with trends in station data (Fig. 7). Additionally the CHIRPS data shows there to be some systematic spatial patterns in rainfall trends, with higher trends along the main N-S axis of the basin, and in the Yom and Wang subcatchments.

There is a clear and statistically significant upward trend in 1981-2019 annual mean and annual mean of minimum temperatures (Fig. 8). Trends in annual mean of maximum temperatures are still upward, but weaker, significant in 12 out of 16 stations.

3.2.2 Extreme rainfall and temperature indices

Trends in extreme rainfall indices are weak, and do not show any consistent sign, nor clear spatial pattern (Fig. 9). In terms of temperature extremes, only trends in tnn (annual minimum value of minimum daily temperature) and txge35 (number of days per year with maximum temperature greater than 35 deg C) are upward and statistically significant (the latter at fewer stations). Station data do not show any trend in txn (annual maximum of maximum daily temperature).

3.2.3 Drought indices

Trends in drought indices evaluated over the 1920-2019 period are in general weak. SPI trends are upward (i.e. towards reduction of drought intensities), but not statistically significant (Fig. 10). Trends in SPEI are, however, downward (i.e. toward increase of drought intensities) and statistically significant in the Yom and Nan sub-catchments (Fig. 11). This demonstrates that drought has tended to worsen only when increases in evapotranspiration are accounted for.

Furthermore, trends in the frequency of drought years show a consistent pattern, particularly for SPEI. Whilst the frequency of drought events defined by SPI on both 12 month and 36 month timescales indicate statistically insignificant trends (Fig. 12), the frequency of droughts indexed by SPEI over the same timescales demonstrates consistent increase, which is statistically significant at 12-month time scales (Fig. 13).

3.2.4 Long-term rainfall variability

Rainfall variability at centennial time scale (1900-2019) in long-term data (CRU, GPCC) is shown in figures illustrating climate projections (Fig. 14). That variability indicates multi-decadal variability, with three phases - an increase in rainfall in the beginning of the 20th century, a decrease in rainfall in the period of 1940-1985, and a rapid increase in rainfall since. Whilst there is a possible plateau or inversion of the trend after ~2005, the observed increase is already as high as the highest estimates from the different multimodal ensemble projections (see discussion below). The station and CHIRPS data capture only the most recent, post-1985 phase, but all the datasets are reasonably consistent in measuring historical rainfall (Fig. 14).

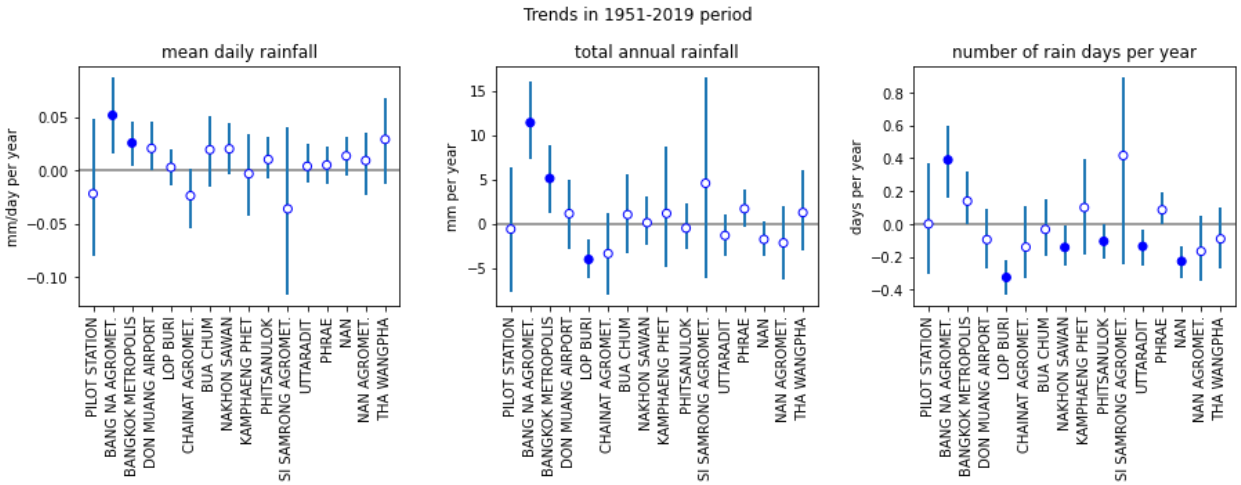

Figure 5: Trends (and their 95% confidence interval) in rainfall attributes in station data. Stations ordered from the most southern to the most northern. Filled symbols - trend significant at 95% level.

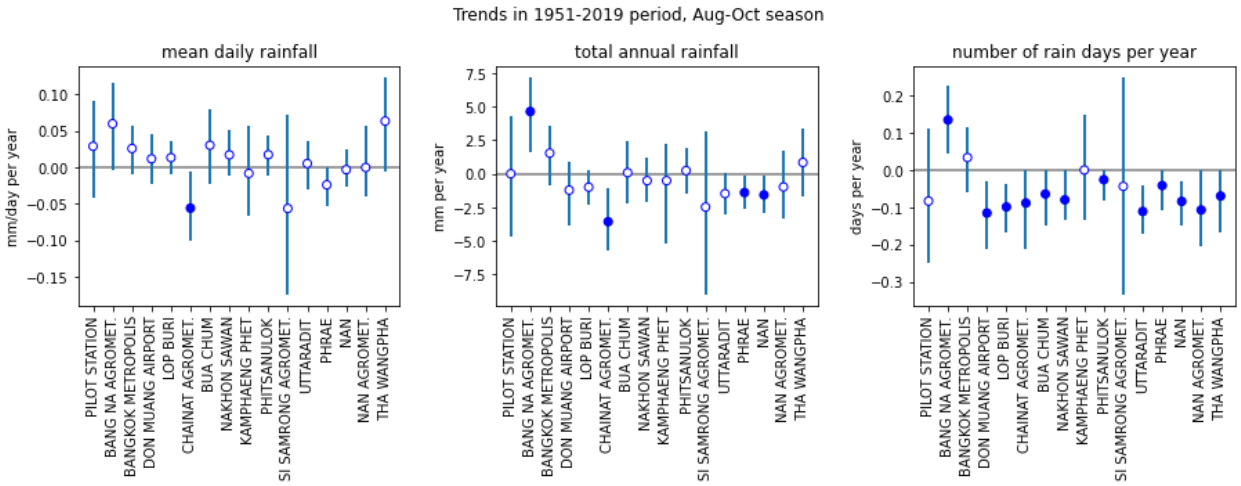

Figure 6: Trends (and their 95% confidence interval) in rainfall attributes in Aug-Oct station data. Stations ordered from the most southern to the most northern. Filled symbols - trend significant at 95% level.

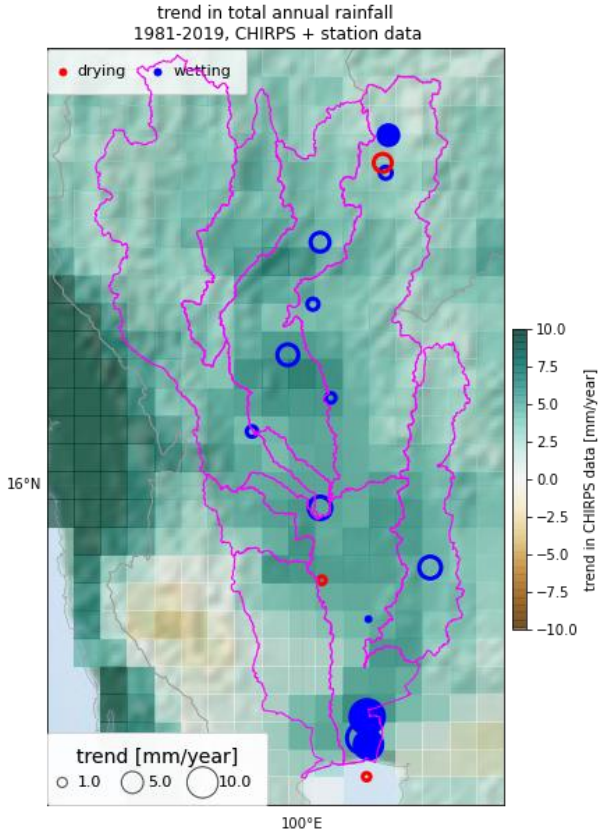

Figure 7: Trends over 1981-2019 in total annual rainfall in station data and in CHIRPS gridded data. Filled symbols - trend significant at 95% level.

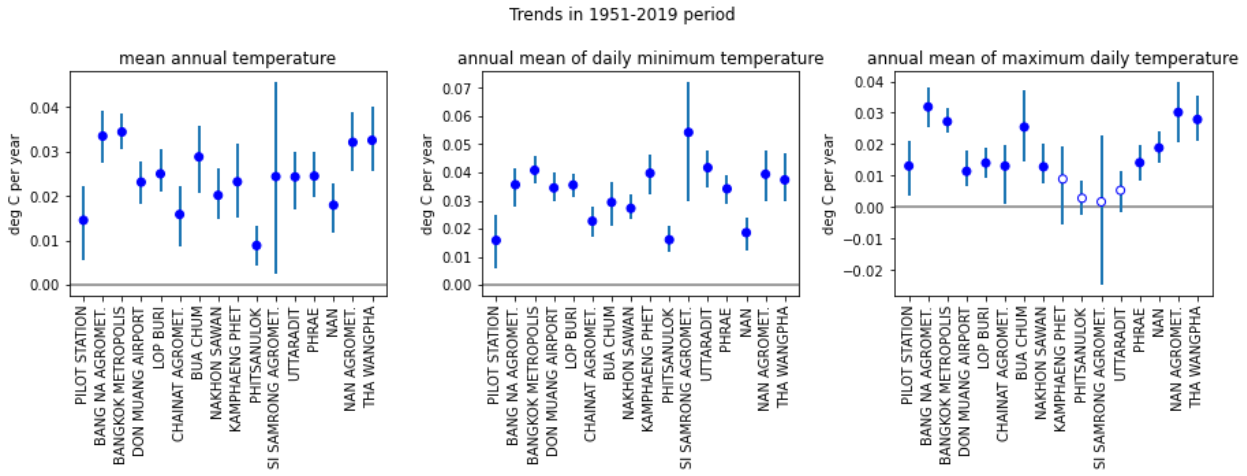

Figure 8: Trends (and their 95% confidence interval) in air temperature attributes in station data. Stations ordered from the most southern to the most northern. Filled symbols - trend significant at 95% level

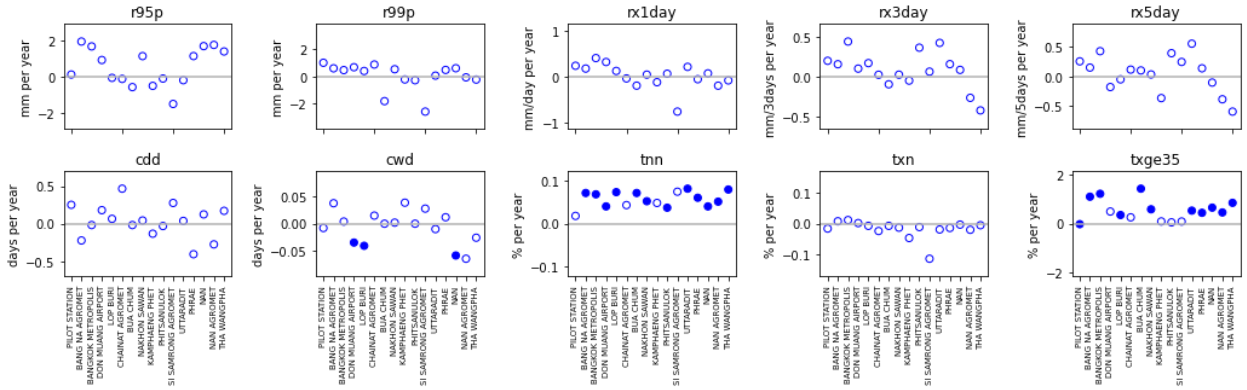

Figure 9: Trends in extreme rainfall indices in station data. Filled symbols - trend significant at 95% level.

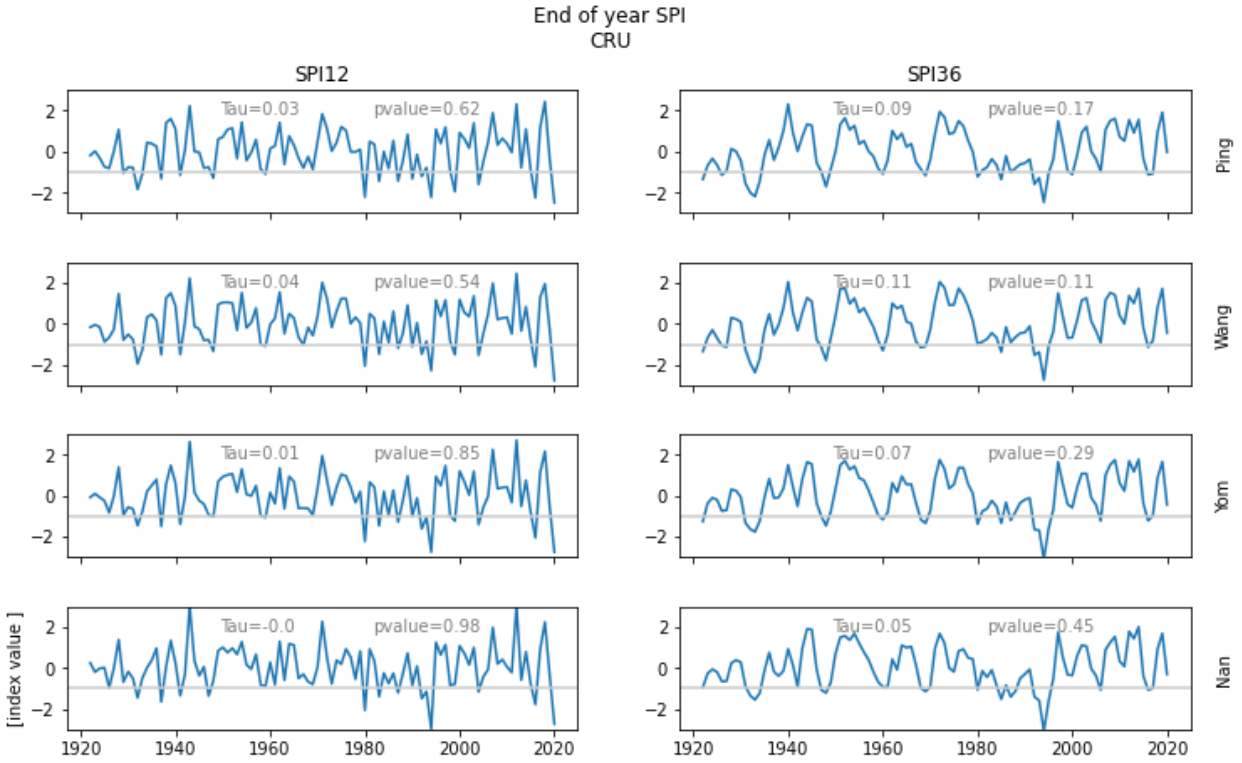

Figure 10: SPI at 12 and 36 months time scale, for individual sub-catchments, based on CRU data. Trend assessed through Mann-Kendall test, with trend significant at 95% level highlighted in bold.

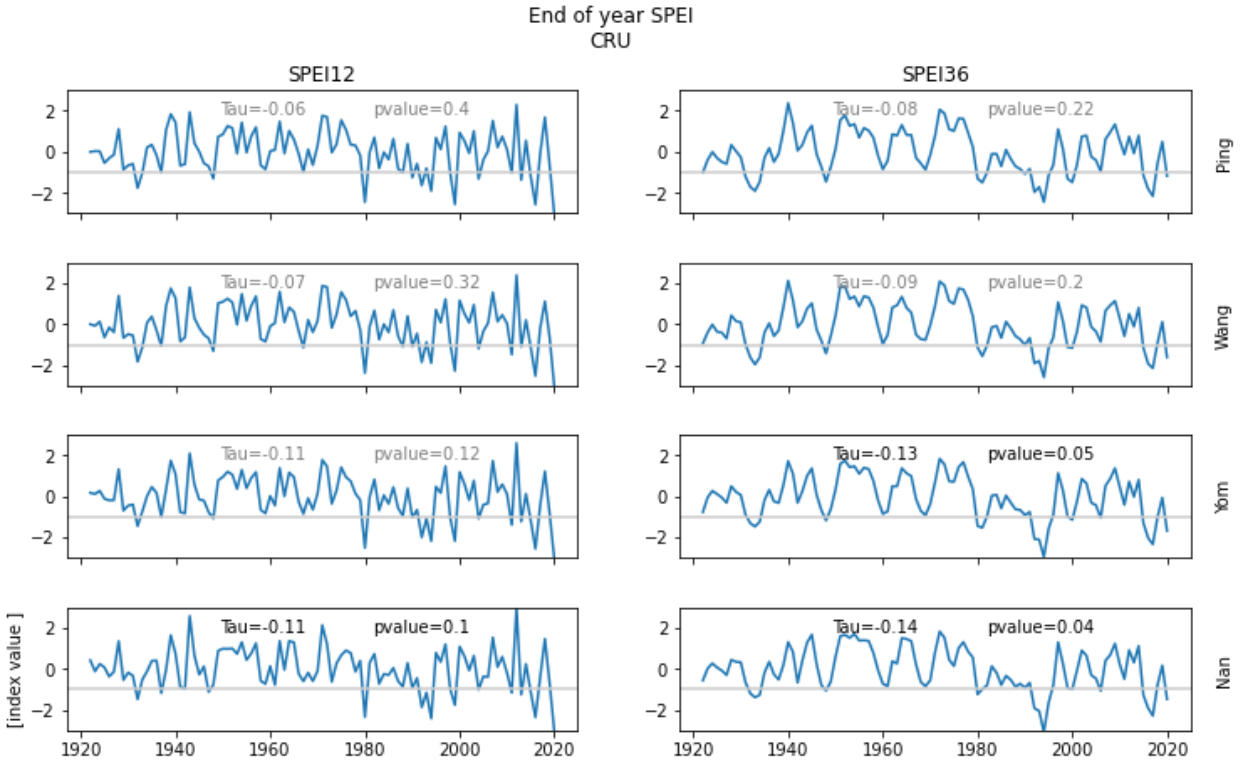

Figure 11: SPEI at 12 and 36 months time scale, for individual sub-catchments, based on CRU data. Trend assessed through Mann-Kendall test, with trend significant at 95% level highlighted in bold.

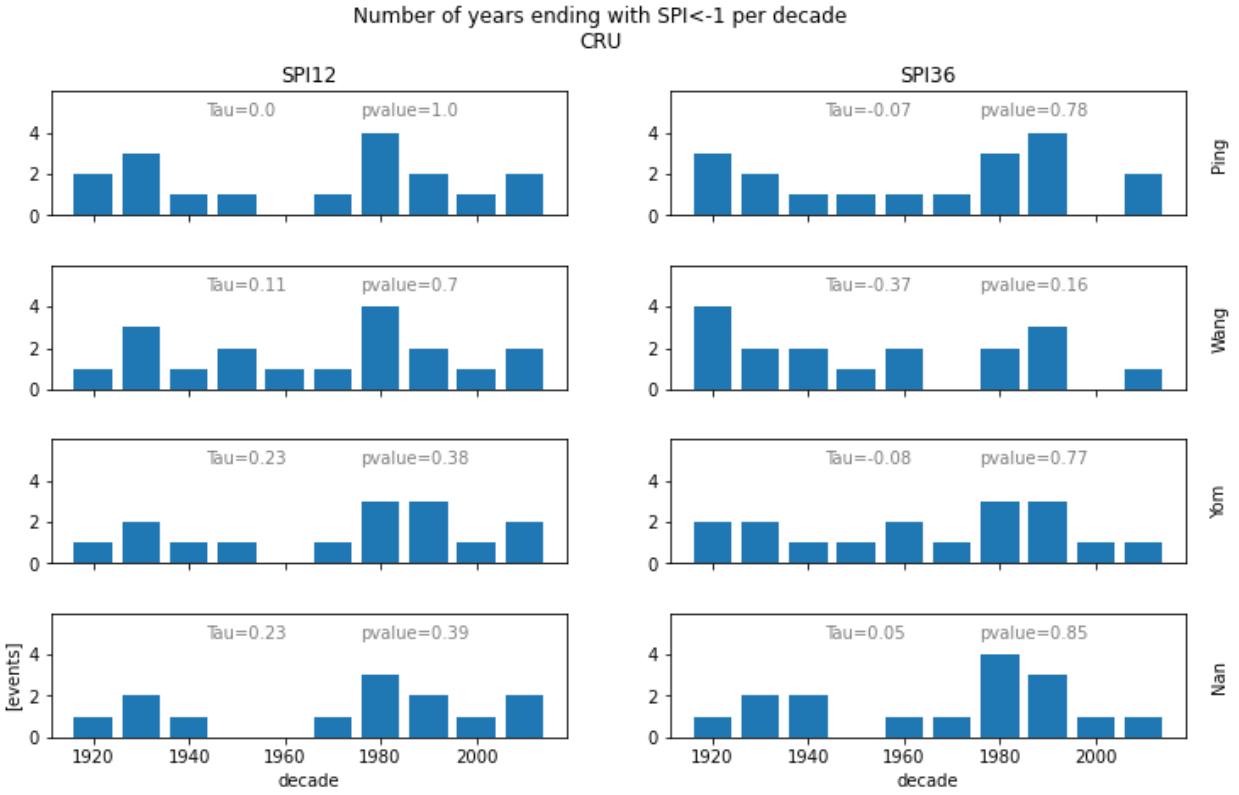

Figure 12: Number of drought years defined by SPI<-1 for 12 and 36-month SPI based on CRU data. Trend evaluated through Kendall Tau with M-K test, when significant highlighted in bold.

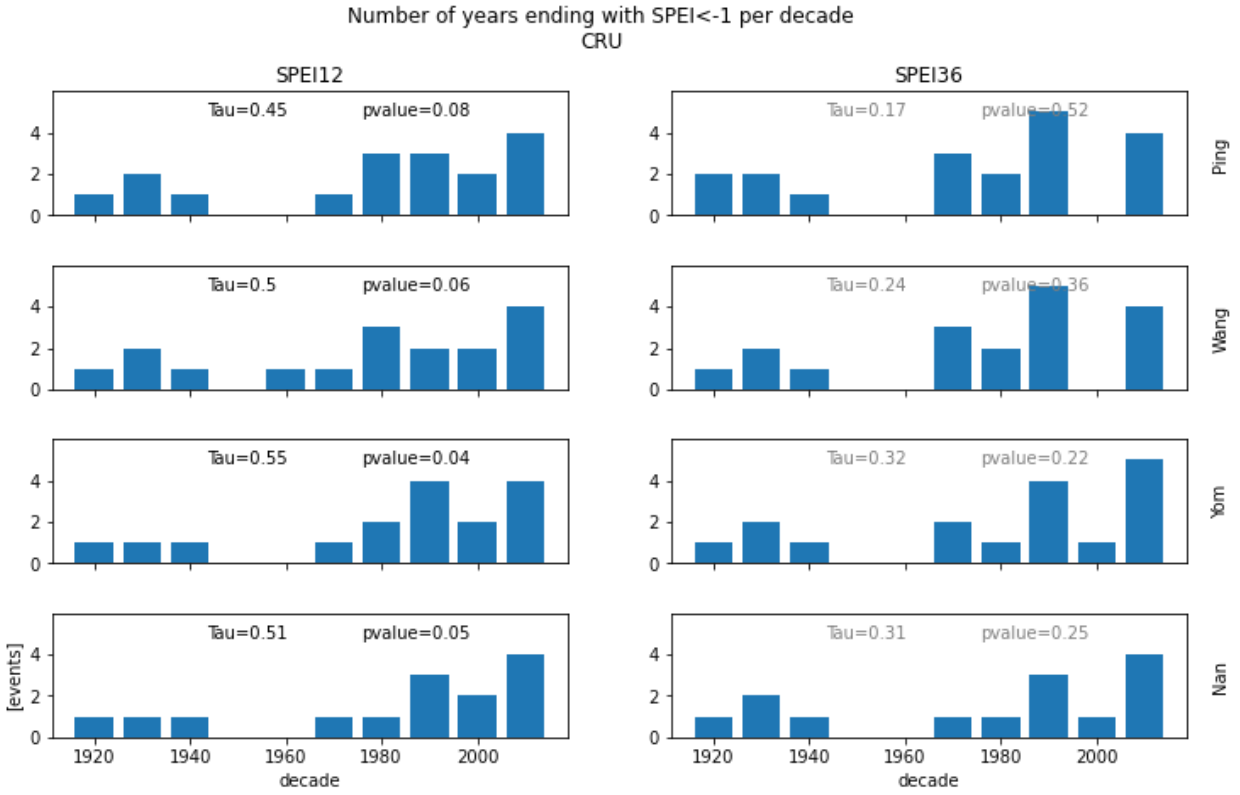

Figure 13: Number of drought years defined by SPEI<-1 for 12 and 36-month SPEI based on CRU data. Trend evaluated through Kendall Tau with M-K test, when significant highlighted in bold.

4 CLIMATE PROJECTIONS

4.1 RAINFALL, TEMPERATURE AND SPEI

We illustrate the multi-generation, multi-model climate projections for the Chao Phraya basin using plume plots (Fig. 14a and b and Fig. 15a and b).

The following observations can be made wrt. projections under the high GHG emission scenario (Fig. 14a and Fig. 15a):

- There are minimal differences between the various sub-catchments.
- There is a good correspondence between the CMIP5 and CMIP6 GCM ensembles. Regional models CORDEX ensemble shows somewhat different pattern to the GCM ensembles, but this is most likely due to the lower number of ensemble members - the CORDEX ensemble has only 7 members (2 RCMs downscaling 3 and 4 GCMs only), while CMIP6 has 24 members for rainfall and 22 members for temperature) and CMIP5 has 37 members. By nature, the smaller CORDEX ensemble is expected to have lower range than the larger GCM ensembles.

- The projections of future rainfall span the range from no-change to increases which steadily progress toward the end of the 21st century, reaching a range of 0 to 25-30% of the 1987-2006 mean.

- Projections of temperature are consistently towards higher temperatures, with the range spanning 2-6 degrees above the 1987-2006 mean at the end of the 21st century.

The projections for the moderate GHG emission scenario are similar in direction to those for the high GHG emission scenario, but lower in magnitude (Fig. 14b and Fig.15b).

We also evaluate occurrence of future drought by calculating 12-month SPEI drought index and calculating decadal count of droughts characterized by index value of -1 or less. We calculate trends in an identical way to that in historical data. Fig. 16 illustrates the results for the Yom sub-catchment under the high GHG emission scenario (other sub-catchments are characterized by similar results). The results indicate the increase in the frequency of 12-month SPEI drought (in 21 out of 22 models), statistically significant in 3 models.

In order to elucidate how the projected increase in rainfall is distributed throughout the season, we calculate relative change in monthly rainfall climatology between the 2051-2080 and 1987-2006 periods. We subsequently apply that relative change to the observed (CRU climatology) to obtain a bias-corrected future climatology for each GCM. Results indicate that the increase in the annual rainfall is mostly driven by the increase in the Aug-Dec rainfall, and that only 2-3 GCMs do not project rainfall increase in that season (Fig. 17). The rainfall change signal in the early rainfall season (Mar-Jun) is less consistent across CMIP6 GCMs, with approx. 50% projecting a decrease.

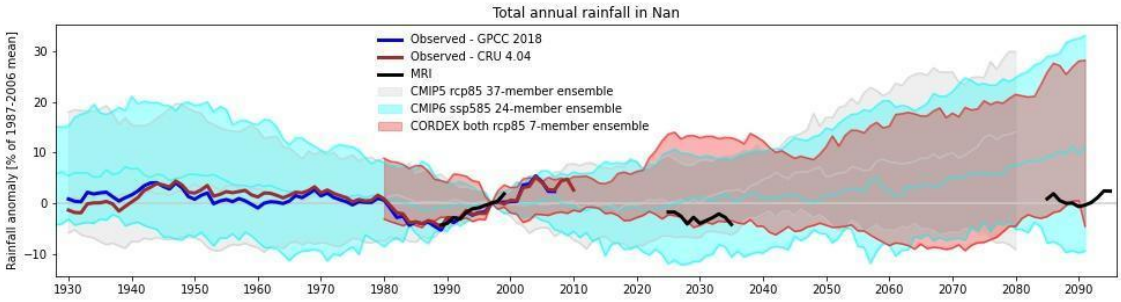

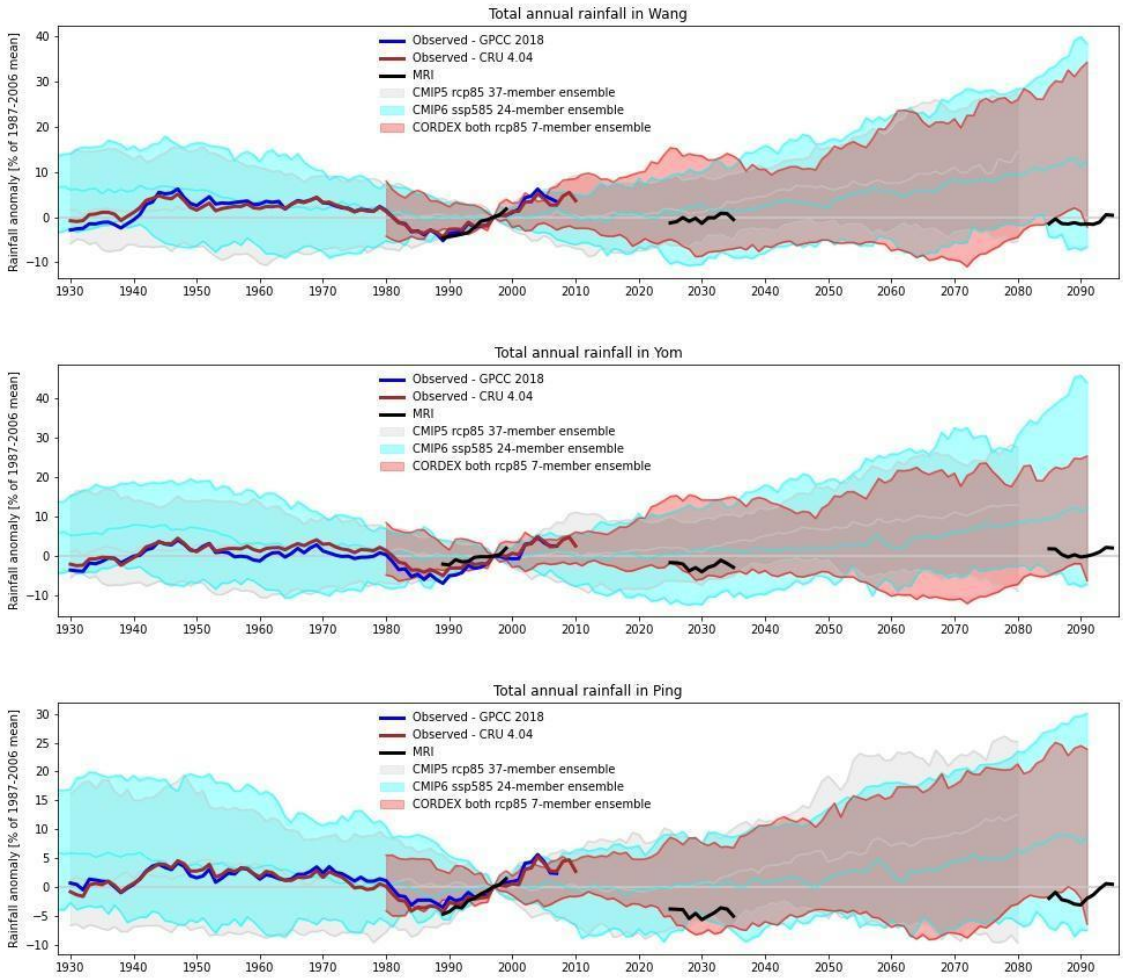

Figure 14a: Historical and projected total annual rainfall under high GHG emissions trajectory (RCP 8.5 and SSP 585), from CMIP5, CMIP6 and merged CORDEX 0.44 and 0.22 deg ensemble. Data from single model projections used in Wichakul et al. 2014 (under SRES A1B) superimposed.

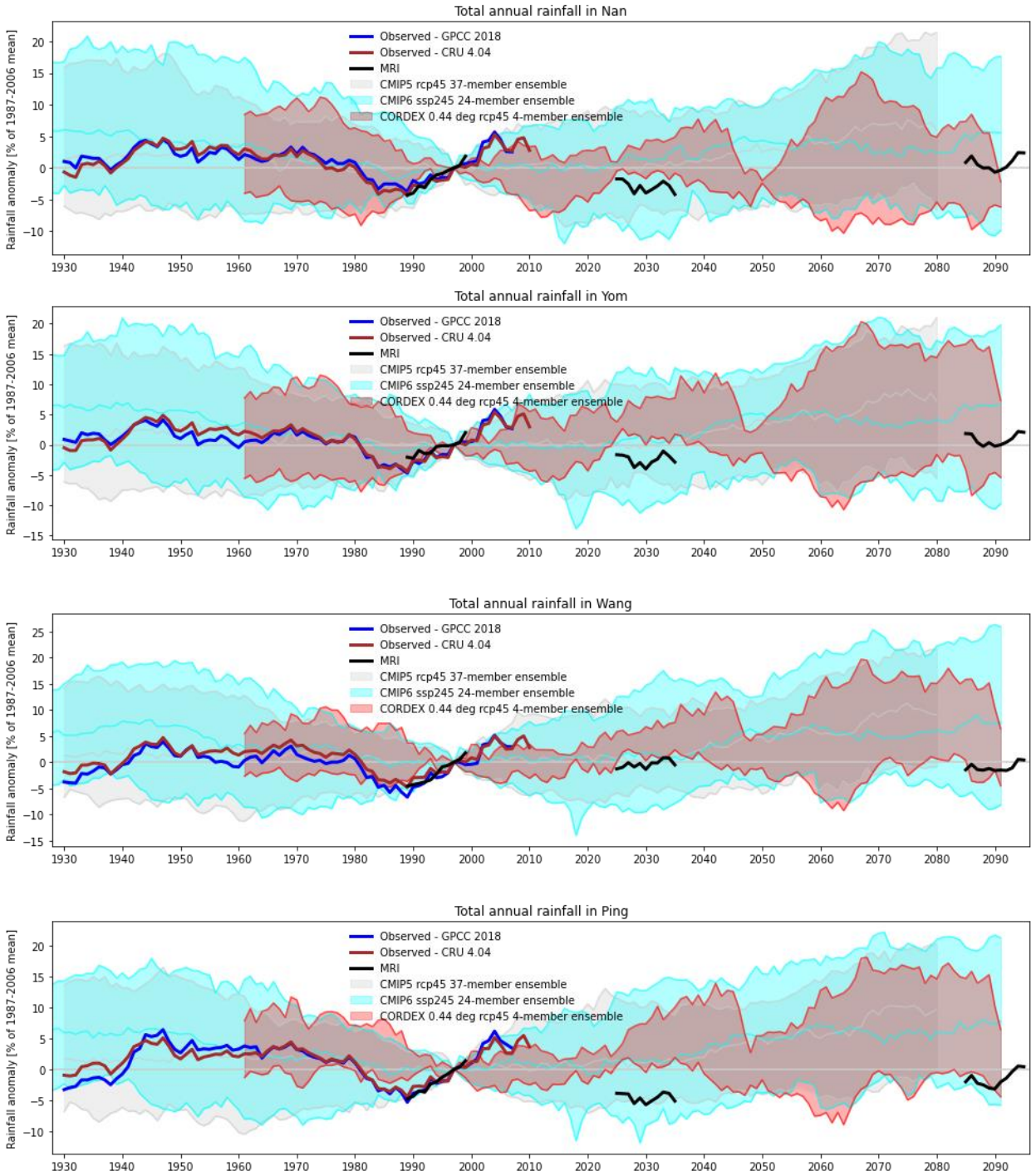

Figure 14b: Historical and projected total annual rainfall under moderate GHG emissions trajectory (RCP 4.5 and SSP 245), from CMIP5, CMIP6 and merged CORDEX 0.44 deg ensemble. Data from single model projections used in Wichakul et al. 2014 (under SRES A1B) superimposed.

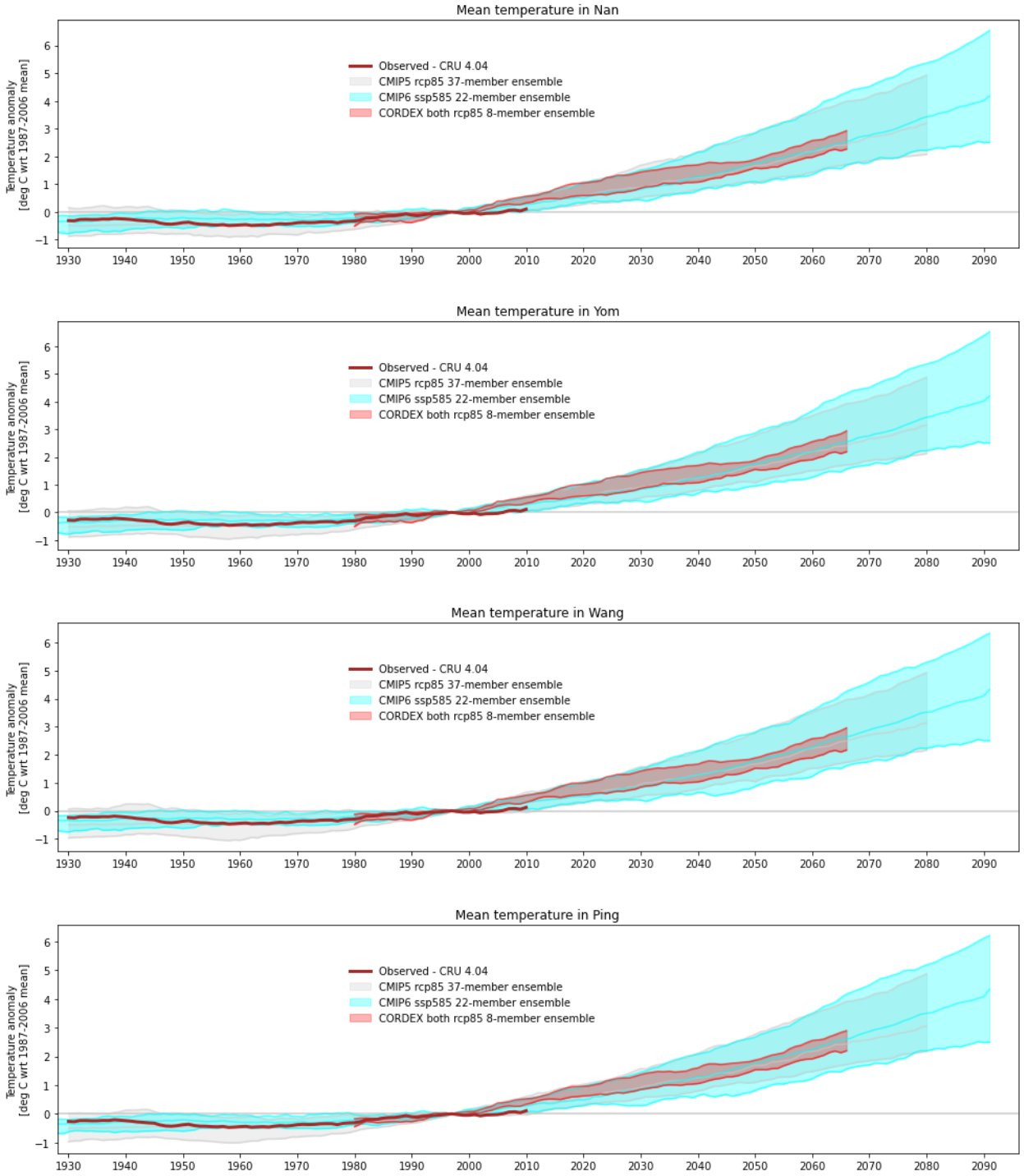

Figure 15a: Historical and projected mean temperature under high GHG emissions trajectory (RCP 8.5 SSP 585), from CMIP5, CMIP6 and merged CORDEX 0.44 and 0.22 deg ensemble

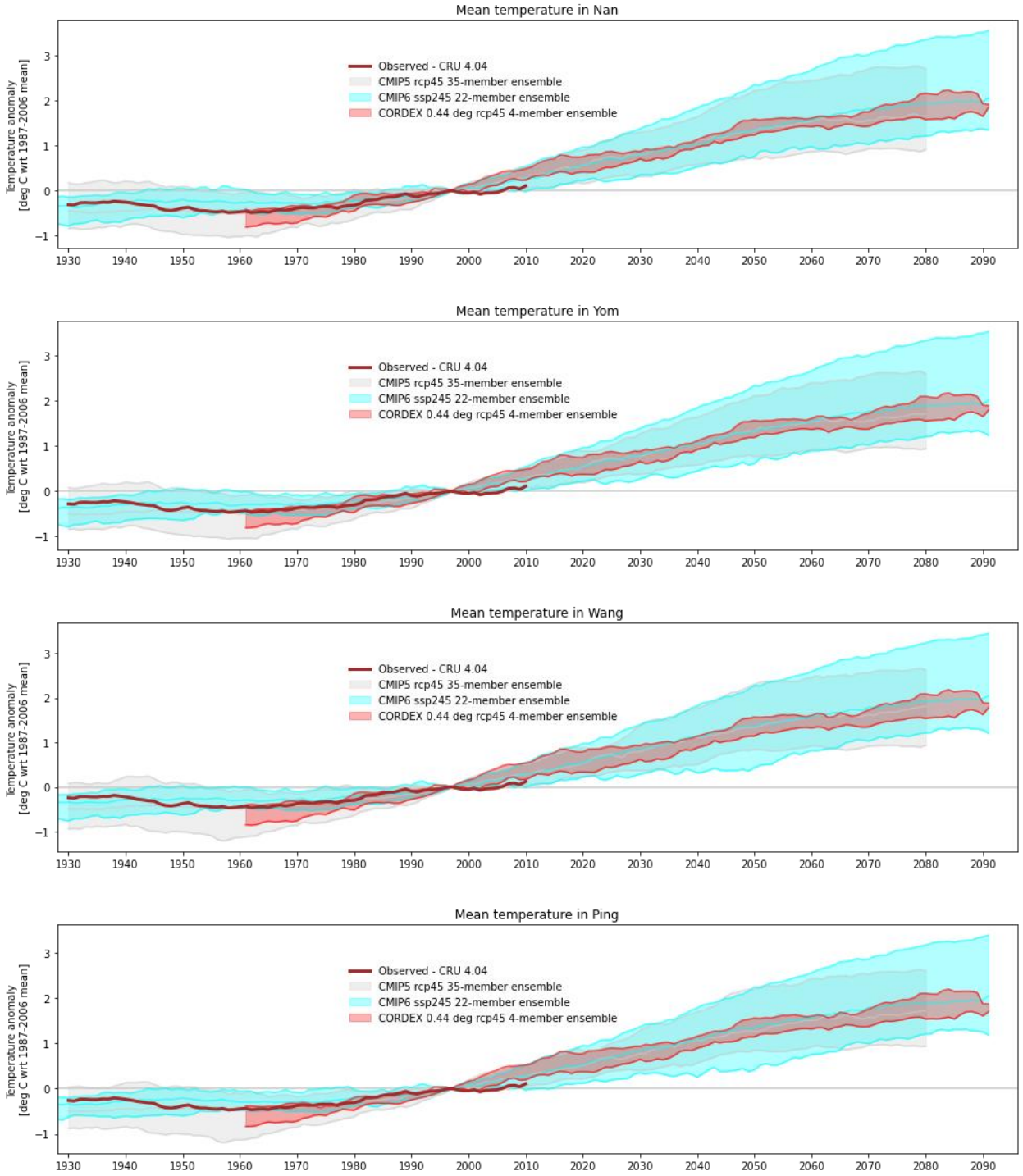

Figure 15b: Historical and projected mean temperature under moderate GHG emissions trajectory, from CMIP5, CMIP6 and merged CORDEX 0.44 deg ensemble

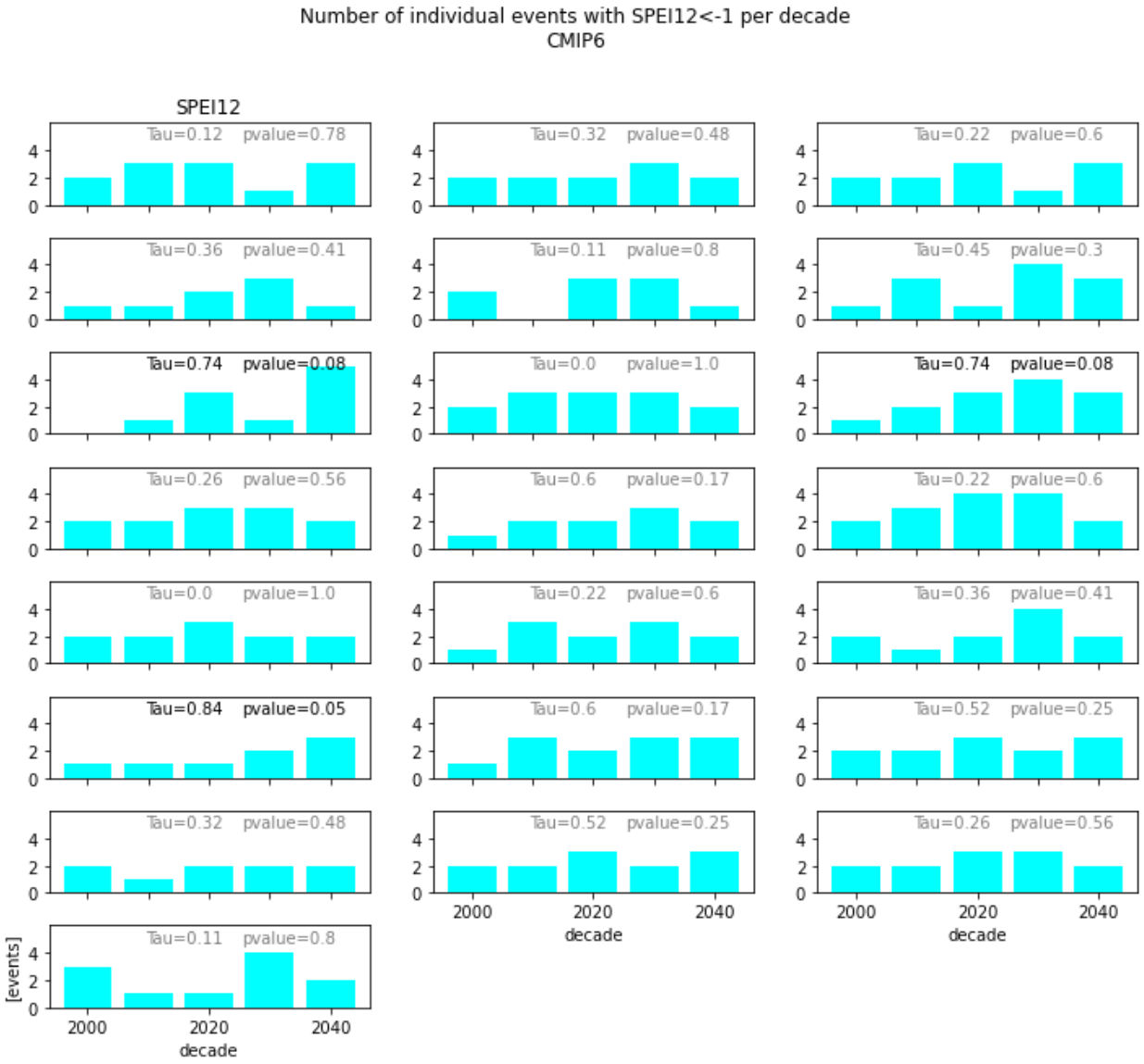

Figure 16: Frequency of drought years, and its trend over 2000-2040 in 22 CMIP6 model simulations for the Yom sub-catchment.

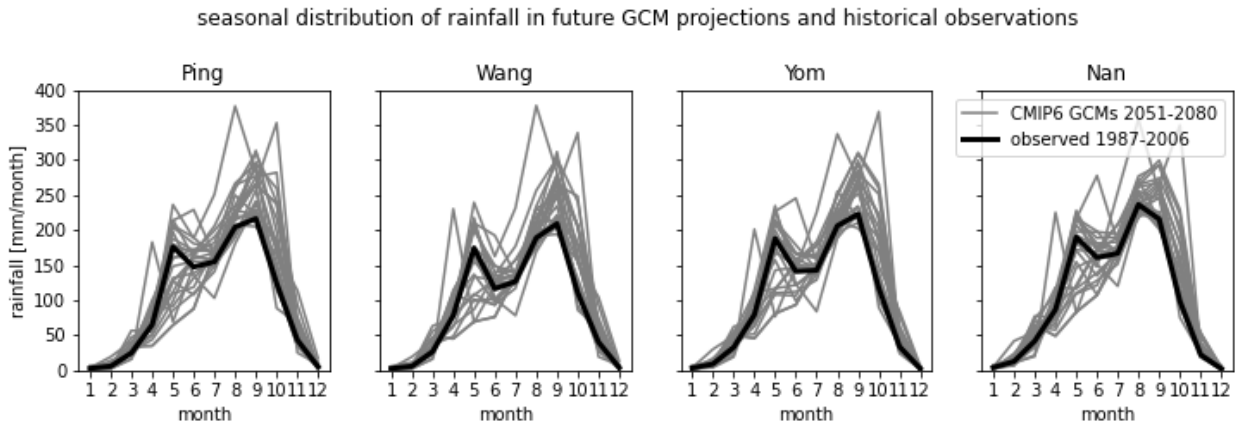

Figure 17: Seasonal distribution of rainfall in GCM projections (bias corrected CMIP6 ensemble) and in historical observations (CRU)

4.2 ARIDITY AND MAXIMUM WATER DISCHARGE

These changes in rainfall, combined with increases in evapotranspiration, will lead to increases in aridity (measured as the ratio of actual evapotranspiration to rainfall) during the dry season and early part of the year (particularly during October and February), with little change during the rainfall season (Figure 18).

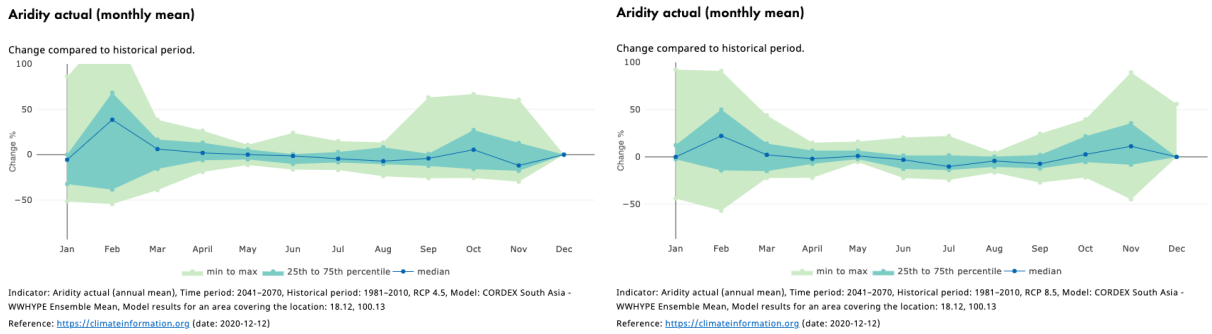

Figure 18: Changes in aridity (ratio of actual evapotranspiration to precipitation) for Phrae (northern Chao Phraya basin) under RCP4.5 (left) and RCP8.5 (right).

Furthermore, the increases in rainfall during the later half of the rainfall season will likely lead to increases in maximum river discharges and hence floods under both RCP4.5 and RCP8.5 in both the near, mid and far future periods of the 21st century (see Figure 19).

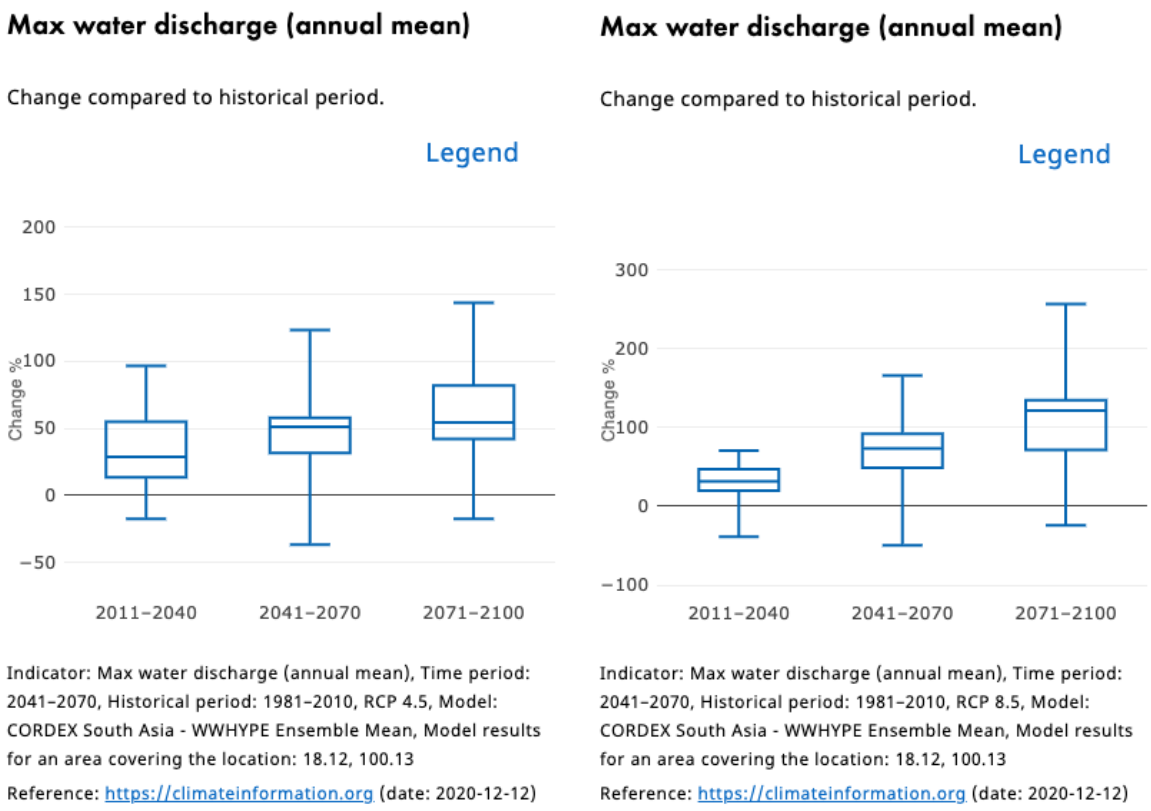

Figure 19: Changes in maximum water discharge at Phrae (northern Chao Phraya) for different future periods under RCP4.5 (left) and RCP8.5 (right).

4.3 CHANGES IN CROP WATER DEMANDS AND IRRIGATION WATER REQUIREMENTS

In order to ascertain implications of anthropogenic climate change on agriculture, as projected by CMIP6 GCMs, we show the historical and projected crop water demand (CWD) defined as CWD=Kc*PET, and irrigation water requirements (IWR) defined as: IWR=CWD-P, where PET is potential evapotranspiration, P is rainfall and Kc is the monthly crop coefficient, depending on the crop growth stage. We use average monthly Kc values for long growth duration rice variety (Hommari 105) to represent rice grown in the Dec-Apr season, and short growth duration variety (RD) to represent rice grown in the May-Jul season (Kc values provided by Dr Akarapon Houbcharaun). The results (Figure 20) indicate that both crop water demand and irrigation water requirement are projected to increase in near future (2021-2050) compared to historical (1987-2006) period. These increases are a result of an increase in PET, that is not compensated by an increase in P, and are simulated by all models in the ensemble. The results, therefore, robustly show that anthropogenic climate change will cause rice to require more water in the future which cannot be met by increases in rainfall alone. Therefore to maintain current rice cropping yields and areas in the basin, under current practices, will require more water or greater efficiencies in the use of water e.g. utilising precision agriculture to reduce water wastage in the application of irrigation.

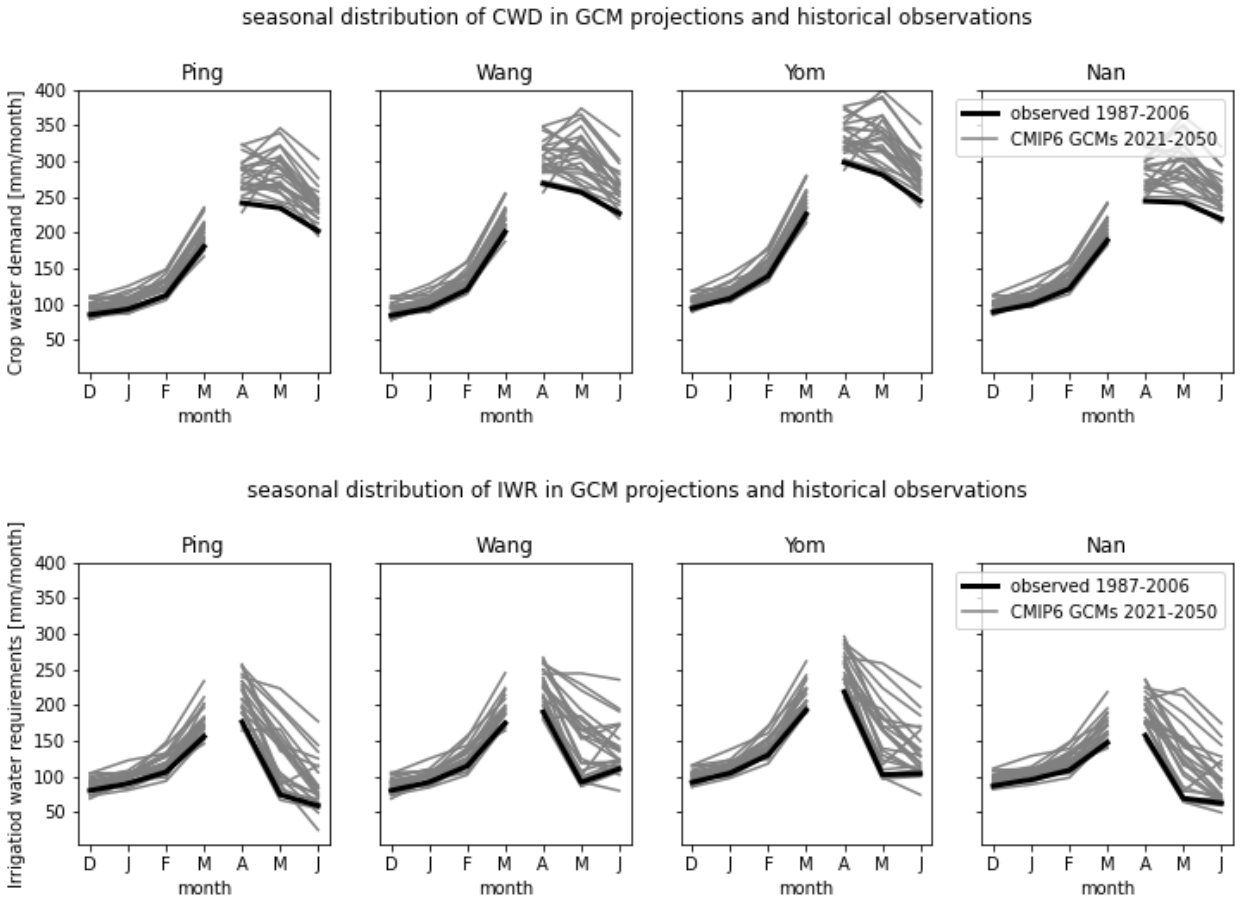

Figure 20 Crop Water Demand (CWD) and Irrigation Water Requirements (IWR) for the two main rice growing season in the analysed region, using Kc values for Hommari 105 rice for the Dec-Mar season and RD rice for the Apr-Jun season. Calculations based on PET derived from air temperature data and precipitation data for each of 22 members of the CMIP6 ensemble under SSP585 emission scenario. Historical values based on CRU data. GCM data are bias corrected in mean so that each individual ensemble members have P and PET (and thus CWD and IWR) identical to observations in the 1987-2006 period.

5 Management of Water Resources in the Chao Phraya basin

Flow in the Chao Phraya River was significantly influenced by the operation of big storage dams in Ping and Nan River basins, named Bhumibol and Sirikit dams, with storage and regulation benefits not only in the Ping and Nan basins, but also for the whole Chao Phraya River Basin including Wang, Yom and Lower Chao Phraya Basins which have total population of 25 million people. Droughts and floods in the Chao Phraya basin are therefore related to reservoir operations and not purely determined by the amount of rainfall or evaporation in the basin. Dams are operated according to the rule curves; upper rule curve (URC) and lower rule curve (LRC), which are generated by using the long term historical data.

The Bhumibol (BB) dam was built in the Ping River basin in 1964 with a capacity of 13,420 billion m^3 and a spillway capacity of 6,000 m^3/s for the purpose of water resources management (irrigation and sea water intrusion protection). Afterwards, in 1974 the Sirikit (SK) dam was built in the Nan River basin with a capacity

of 9,510 billion m^3 and spillway capacity 3,250 m^3/s, mostly for irrigation. The catchment areas of the BB and SK dams are 26,400 km^3 and 13,130 km^3 respectively.

Figure 21 and 22 present the volume of the reservoir and operation rule curves of the Bhumibol and Sirikit dams, respectively. These figures show some of the intra-annual and inter-annual variability in the water available in the basin. In 2011 a devastating flood caused by continuous intense precipitation occurred, both dam water levels are higher than the upper rule curve. In 2018 the water availability was quite low and met the lower rule curve for both dams. In 2019 and 2020 the water volume for both dams are extremely low and meet the dead storage level. Figure 23 and 24 illustrate inflow to dams since both dams have been in operation. The graphs show that high inflow begins from July and lasts until November. This is different to the situation without the dams, where inflow according to rainfall in Nan river basin peaks earlier in June and later in August-October.

The Royal Irrigation Department announces plans for reservoir water resources management on a seasonal basis. For example, for rainy season 2019, water releases were planned for May-October of approximately 2,550 MCM (1,000 MCM form BB dam and 1,450 MCM from SK dam), and for dry season 2019/2020 water releases were required during November-April which have total amount of approximately 3,050 MCM (1,200 MCM from BB dam and 1,850 from SK dam). [Ref: http://hydro-5.rid.go.th/]

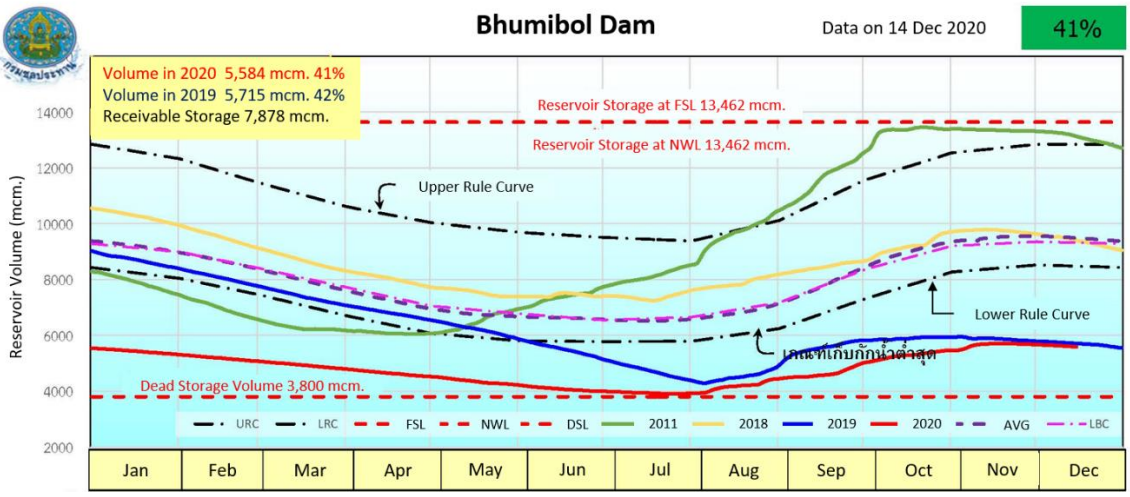

Figure 21: Reservoir Volume and Operation Rule Curves of the Bhumibol Dam in Ping River Basin

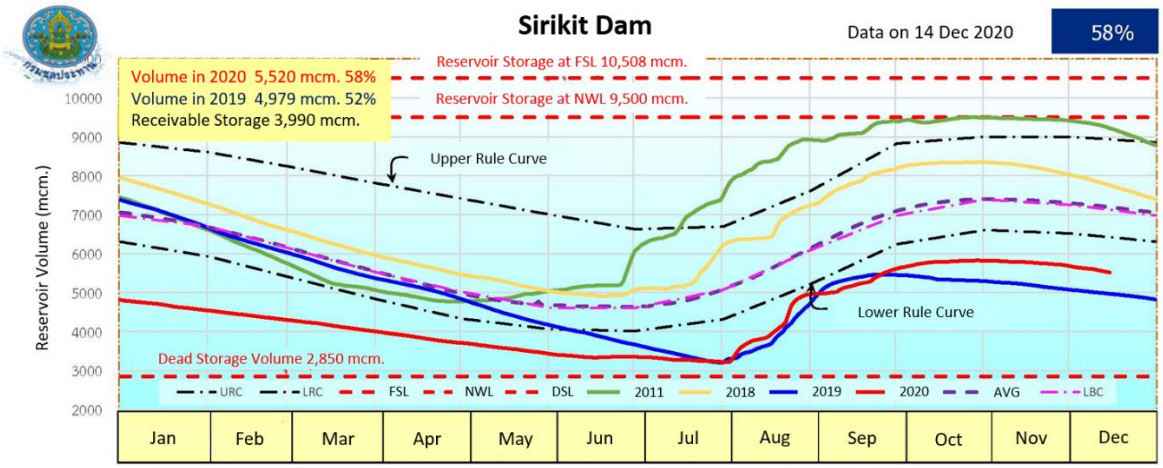

Figure 22: Reservoir Volume and Operation Rule Curves of the Sirikit Dam in Nan River Basin

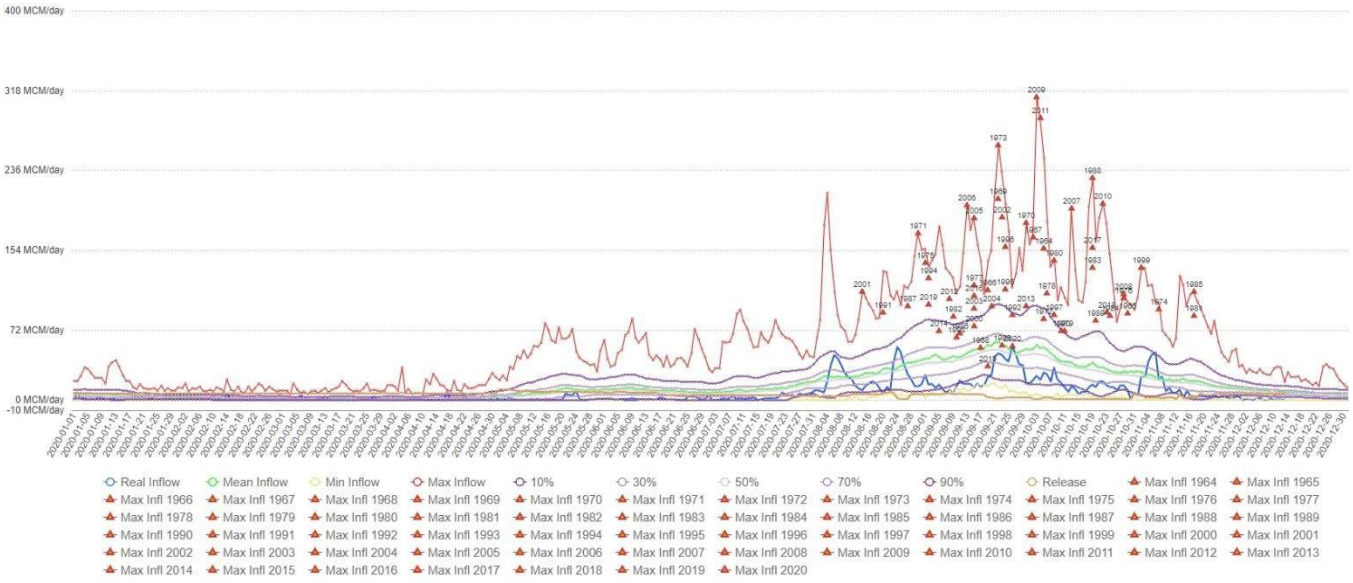

Figure 23: Inflow 2020 to Bhumibol Dam in Blue Line (recorded data 1964-2020)

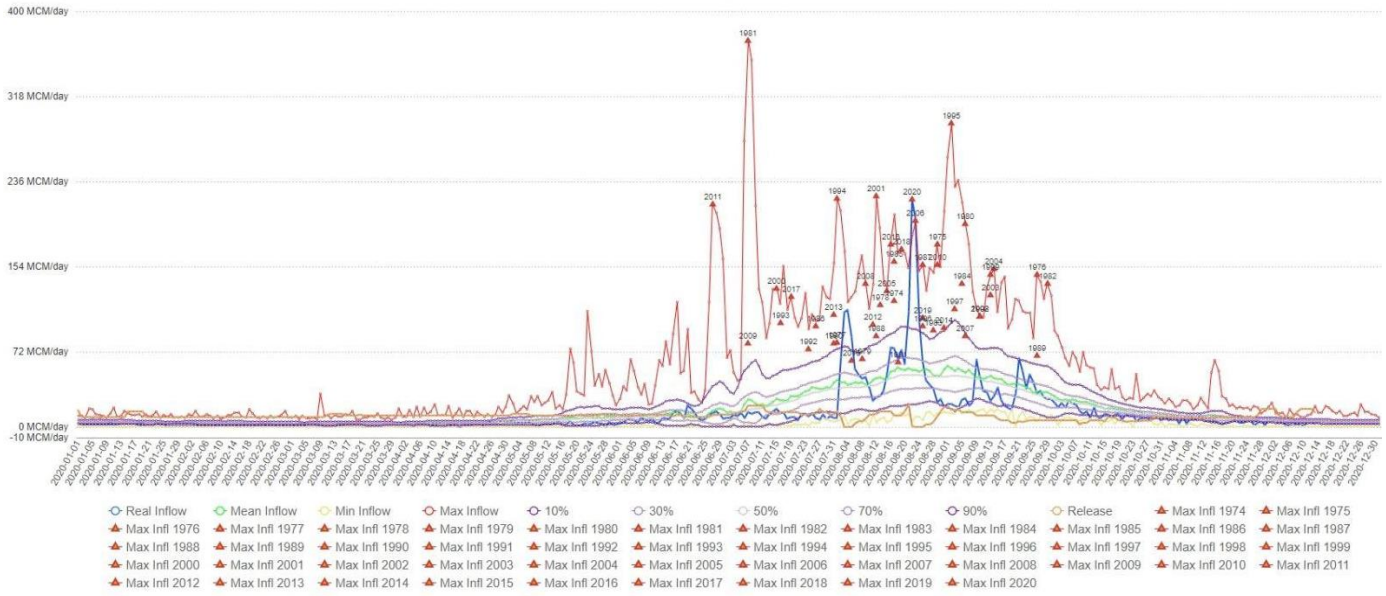

Figure 24: Inflow 2020 to Sirikit Dam in Blue Line (recorded data 1974-2020)

6 HYDROLOGICAL IMPACTS AND MITIGATION OF CLIMATE CHANGE IN THE CHAO-PHRAYA BASIN

6.1 HYDROLOGICAL IMPACTS

Wichakul et al. (2014) conducted a baseline study for Chao Phraya basin (Ping, Nan, Yom, and Wang sub-basins), evaluating hydrological impacts of climate change on streamflow in that basin. They utilized a bespoke comprehensive distributed hydrological model that accounted for rainfall-runoff processes, flood wave propagation processes as well as water management activities and water abstractions in the basin. The model has been calibrated against observed river discharges.

The study utilized climate projection from a single global climate model: MRI-AGCM3.2s with spatial resolution: ~20km. The projection was modelled under SRES A1B GHG emission scenario, which is non-conservative ("worst case") used in the CMIP3 global climate modelling experiment.

In that study, GCM rainfall and potential evaporation data were bias corrected to observations, and the hydrological model was used to simulate three continuous periods: historical (1979-2007), near future (2015-2044), far future (2075-2104).

Results were presented in terms of impacts at the outlet of the basin at C2 gauge (thus combining all 4 sub-catchments). The study demonstrated (see Figure 25):

- an increase in mean annual discharge in both near and far future,

- a decrease in flows during the low flow period in near future,
- an increase in flooding frequency in both near and far future.

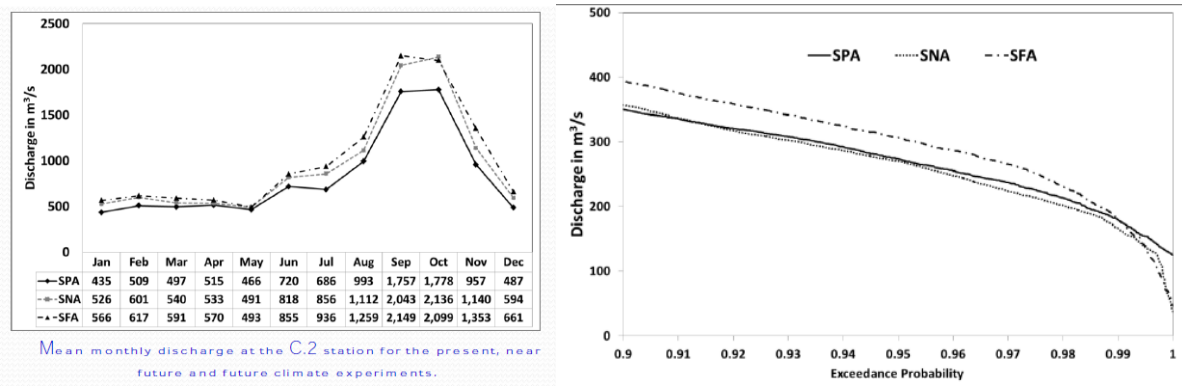

Figure 25: Historical and projected discharges of Chao Phraya River based on MRI-AGCM3.2s under SRES A1B scenario (Wichakul et al. 2014).

Since the Wichakul et al. 2014 results are based on a single GCM projection, there is a need to contextualize those results within the broader landscape of multi-generation, multi-model projections considered here. In order to illustrate how the MRI-AGCM3.2s rainfall projections relate to the other models/ensembles used here, we superimposed the sub-catchment average rainfall figures from that model onto the plume plots in Fig. 14. As that figure illustrates, the MRI-AGCM3.2s projection is a moderately "dry" projection in the near future, and is one of the "driest" projections in the far future. In other words, approx. 60-75% of ensemble members of CMIP5 and CMIP6 ensembles simulate wetter near future than MRI-AGCM3.2s, while for the far future, that number is about 90%. This is consistent with the results of Kotsuki et al. (2014) who demonstrated that a suite of 6 CMIP5 GCMs all simulate increases in average runoff over the Chao Phraya basin under both RCP4.5 and RCP8.5, for both near (2040-2059) and far future (2080-2099) periods during the 21st century (Figure 26). Only the CSIRO GCM under RCP4.5, and IPSL (near future RCP4.5 and far future RCP8.5) indicate small regions towards the north east of the basin that will likely have decreases in runoff. This study estimates large increases in runoff (>20%) under both RCP scenarios at C.2 (beginning of Chao Phraya river) due to increases in mid-season rainfall (Figure 27). Increases in annual runoff in the C.2 catchment were 45.8 mm (5.0 x10^9 m^3) and 85.4 mm (9.4 x10^9 m^3) under the near-future climate scenario, and 83.9 mm (9.2 x10^9 m^3) and 129.5 mm (14.2 x10^9 m^3) under end-of-the-21st-century climate scenario, for RCP 4.5 and RCP 8.5, respectively. Compared to the capacities of the Bhumibol and Sirikit dams (13.5 and 9.5 x 10^9 m^3), projected increases in runoff at the end of the 21st century are high and will likely require new flood management and mitigation plans, including the construction of new dam reservoirs and changes in the rules for operation of dam gates.

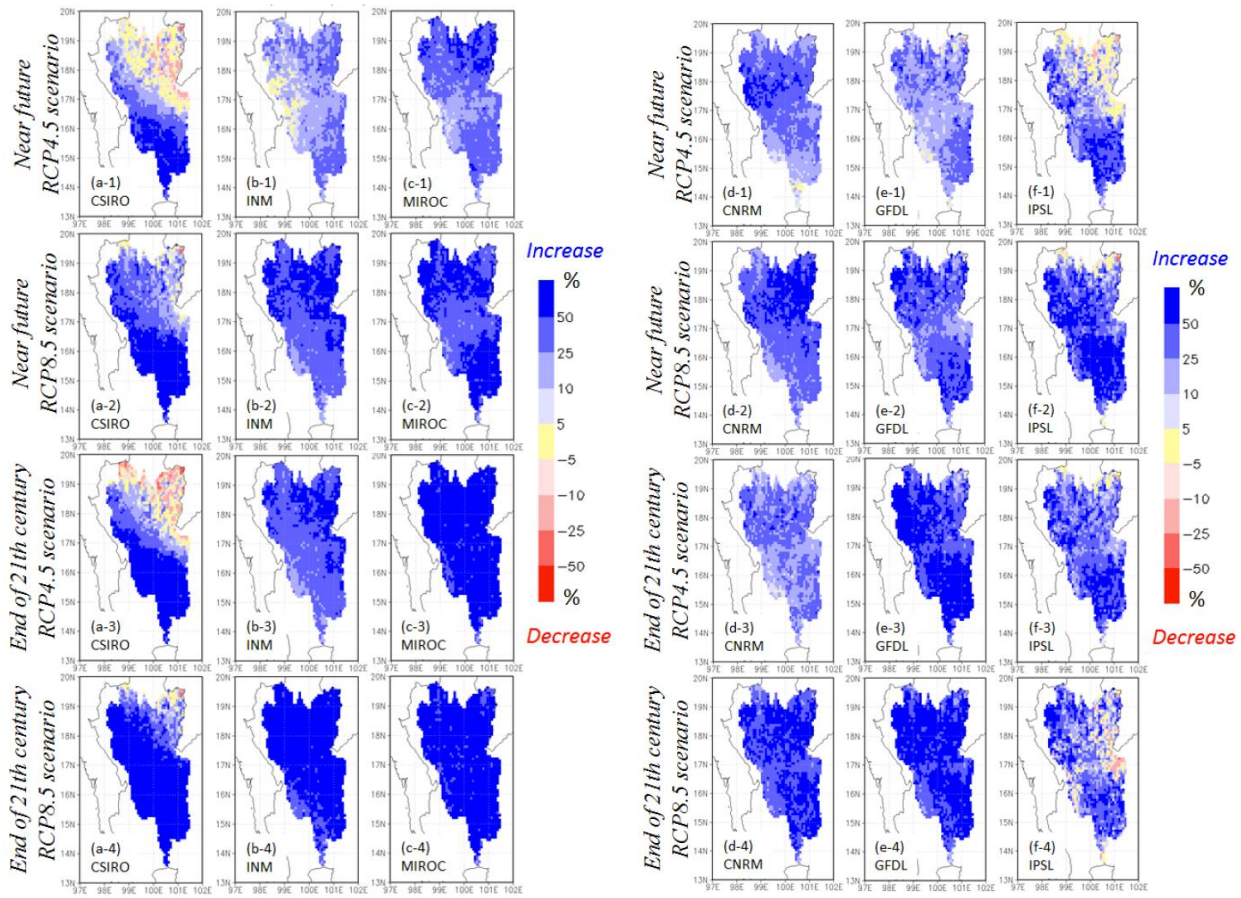

Figure 26: Climatological annual mean runoff change (%) in the future climate relative to the present climate. Top figures (a-1, b-1, c-1, d-1, e-1 and f-1) show projected near-future (2040–2059) change under the RCP 4.5 scenario. Second top figures (a-2, b-2, c-2, d-2, e-2 and f-2) show projected near future changes under RCP 8.5 scenario. Third top figures (a-3, b-3, c-3, d-3, e-3 and f-3) show projected end-of-21st-century (2080–2099) changes under the RCP 4.5 scenario. Bottom figures (a-4, b-4, c-4, d-4, e-4 and f-4) show projected end-of-21st-century changes under RCP 8.5 scenario. Figures a1-a4, b1-b4, c1-c4, d1-d4, e1-e4 and f1-f4 were calculated with CSIRO, INM, MIROC, CNRM, GFDL, and IPSL, respectively. Cold and warm colors represent increase and decrease, respectively. From Kotsuki et al. (2014).

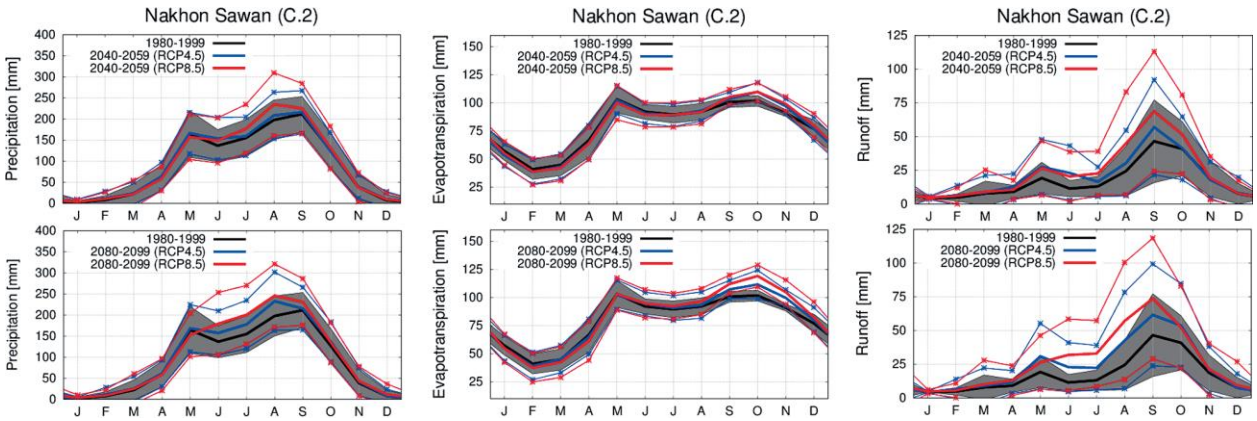

Figure 27: Comparisons of monthly precipitation (a-1, a-2), evapotranspiration (b-1, b-2), and runoff (c-2, c-2) in Nakhon Sawan catchment. Panels a-1, b-1, and c-1 show comparisons between present climate (1980–1999) and near-future climate (2040–2059). Panels a-2, b-2, and c-2 show comparisons between present climate and

end-of-21st-century climate (2080–2099). Solid black lines and gray shaded areas show averages and standard deviations for the present climate. Solid blue lines and blue lines with x-marks show averages and standard deviations under the RCP 4.5 scenario. Solid red lines and red lines with x-marks show averages and standard deviations under the RCP 8.5 scenario

In order to further explore the climatic drivers of the relatively strong impacts on the discharges of the Chao Phraya River, we have analysed sub-catchment rainfall climatology in the MRI-AGCM3.2s data in the historical, near future and far future periods (as in Wichakul et al. 2014). Results, illustrated in Fig. 28 show that rainfall change in both "futures" are relatively minor, but there is a relatively consistent increase in total rainfall in the Jul-Sep period, driven by changes in rainfall intensity. These changes in seasonality are consistent with the multimodal ensemble shown in Figure 17, and as stated above it is reasonable to assume that forcing from other GCMs would produce similar, if not greater, increases in discharge and flooding.

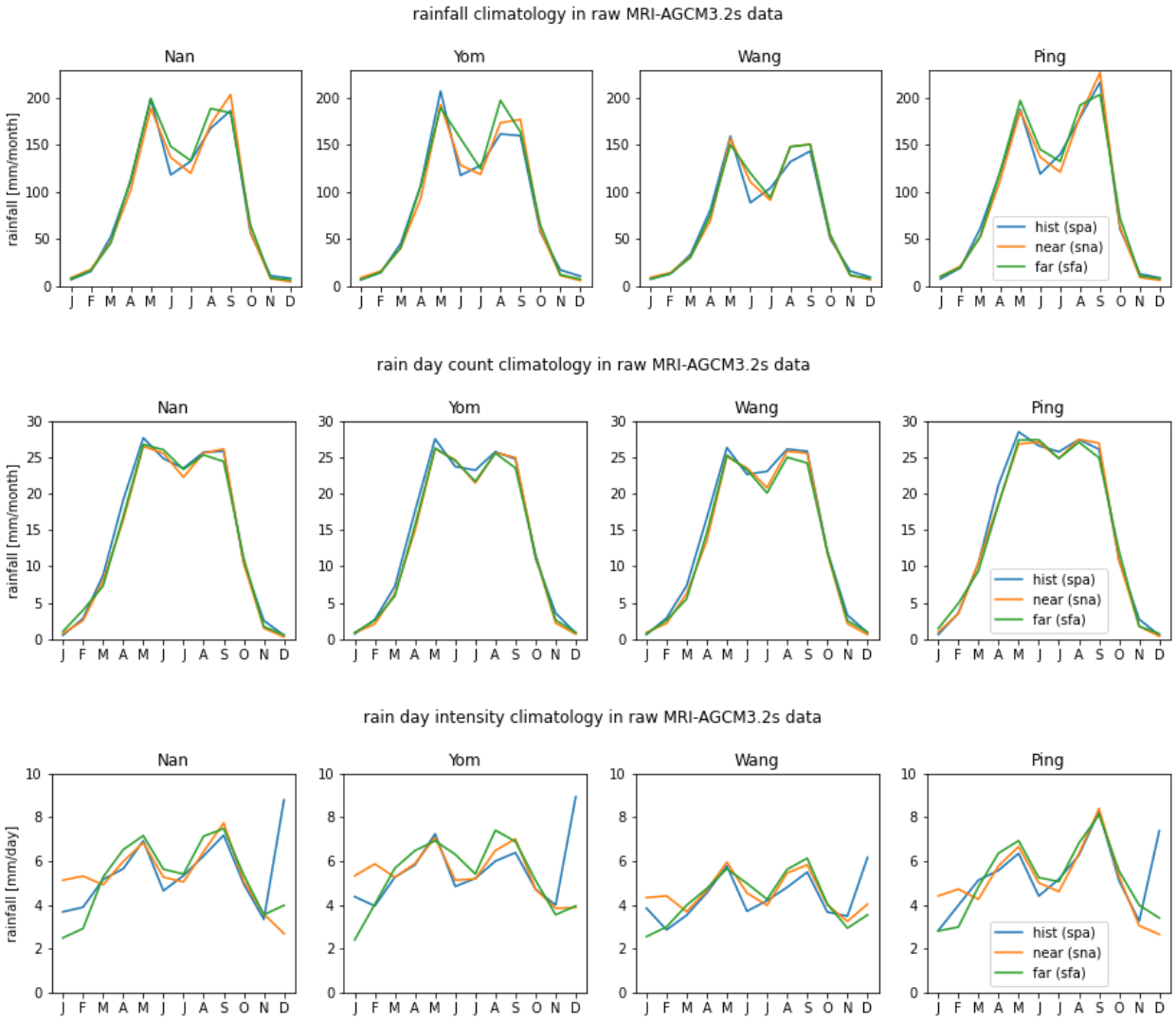

Figure 28: Rainfall (total, rain day count and rain day intensity) climatology in raw MRI-AGCM3.2s data.

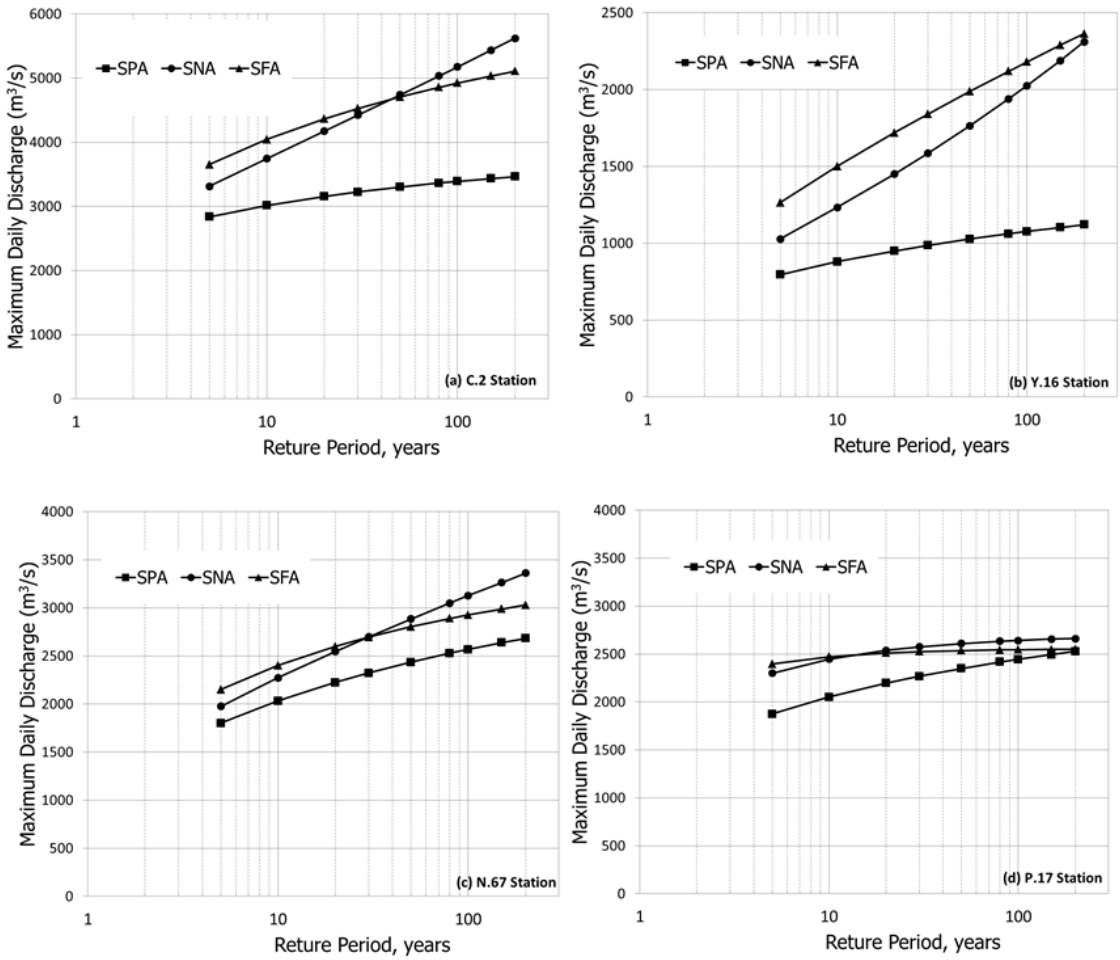

Figure 29: Maximum daily discharge corresponding to different return periods for present climate (SPA), near future climate (SNA) and future climate (SFA) for each location.

A frequency analysis of extreme projected discharges by using the MRI-AGCM3.2s (Wichakul et al. 2014), shows changes in maximum daily discharges for different return periods and are illustrated in Figure 29 for four different locations; (a) for C.2 station the beginning of Chao Phraya River, (b) for Y.16 station at the outlet of Yom River, (c) for N.67 station at the outlet of Nan River and (d) for P.17 at the outlet of Ping River station. The assessment has been conducted by comparing the return period of the 5-year, 10-year, 20-year, 30-year, 50-year, 80-year, 100-year, 150-year, and 200-year discharges. Shorter return periods (shorter than 50-years) affect flood related design structures, such as irrigation structure, urban drainage and bridges. Figure 29a, demonstrates that during the 21st century the magnitude of extreme events at the C.2 station significantly increase for return periods shorter than 50-years and also it is larger than the magnitude of discharges in the near future climate (2015-2043). For long return periods (> 80-years), the magnitude of discharge is extremely high in the near future climate. That change in the C.2 station mostly corresponds to change in flood magnitude in the P.17 and N.67 stations for both near future and future periods (Figures 29c and 29d). Flood frequency

analysis of the Y.16 station showed different patterns from other locations, as illustrated in Figure 28b because the location of the Y.16 station is far for the location of the other three stations. Flow from the Y.16 station merges with the Nan river at the confluence located upstream of the N.67 station. The corresponding discharge of the C.2 station (5,034 m^3/s) at 80-year return period of the near future is larger than the peak discharge of Thai's flood 2011 (4,686 m^3/s). Consequently, the simulated discharges shows that flood risk will increase in the future, likely at a scale/level greater than seen in 2011.

6.2 MITIGATING FLOOD RISKS

Given the results of the modelling above and the uncertainty associated with future projections of rainfall it is recommended that interventions to mitigate flood risks be based on current flood risks, known areas where flooding risks pose a threat, and to the extent possible allow for flexibility to adapt to changes in future rainfall distributions and flooding as they evolve.

As part of the 2012 Master Plan on Water Resource development the responsible consulting firms prepared a flood risk map which RID use as reference for planning. Figure 30 shows this map which utilised current climate conditions and the MIKE Flood model (hydrodynamic) and MIKE Basin model (water balance) to identify the current risk of flooding. The proposed infrastructure target sites are based on both the current flooding risk (Figure 30), the current stream and drainage system, and analyses utilising the concept of 'Monkey cheeks', which represent areas where water is retained upstream to prevent flooding downstream (see below). Whilst there is no one model or methodology to identify the required infrastructure and target areas, there is clearly a need to improve RID's capacity to undertake these assessments as part of their planning process, and the GCF project can help this goal by investing in developing hydrological modelling capacity at RID.

Furthermore, RID engineers do site selections in consultation with water users, which once agreed and finalised allow construction plans to be developed and presented to the River Basin Committee. The annual budget for hard infrastructure in each location needs approval of the Sub-committee on Provincial Water Resources that consist of local administrations, water users (farmer, industrial, resident). These consultations are extensive and require a recognition of existing power imbalances to be effective (Trakuldit and Faysse, 2018).

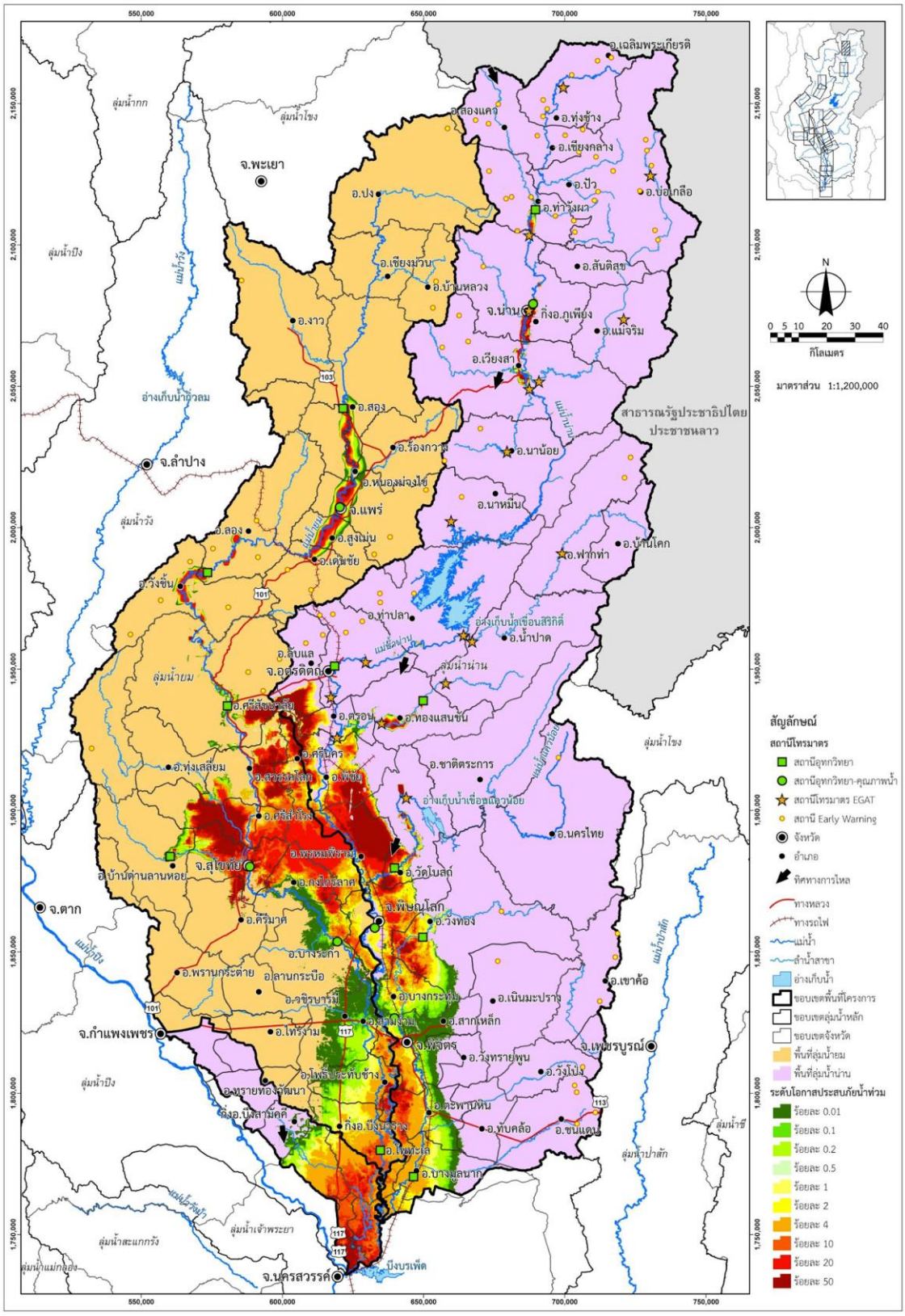

Figure 30: Current flood risk and location of the 13 proposed grey infrastructure sites (green squares).

The concept of "Monkey Cheeks" was introduced by Thailand's late King RAMA IX who was an Irrigation Engineer. He guided RID to adopt a concept of nature-based solutions in which the Monkey Cheek concept refers to water retention and detention approaches for flood prevention. The feasibility assessment for "Monkey cheek in lowland area above Nakhon Sawan province" did hydrological modelling to analyse the six phases of flood retention areas which should be built in the Yom-Nan river basin. As noted above the 13 schemes were chosen partly based on this modelling and used this information to guide their Operation & Maintenance Plan. The 13 proposed schemes comprise of existing regulators/flood gates which have been built 10-20 years ago and whose efficiency is low. RID propose to upgrade these existing regulators/floodgates and improve the condition of irrigation canals and their capacity to enable the monkey cheek concept e.g. dredging of canals, maintenance and improvement of existing weirs and diversion structures, heightening embarkments and dams, and constructing new retention ponds within the protect area. This was to be for the 13 schemes to be improved one location per year, over a 13 year period (Business as Usual). However, with GCF funding the O&M plan to complete these 13 schemes can be completed in a shorter period of time.

6.2.1 IDENTIFICATION OF 13 INTERVENTIONS

The improvement of existing irrigation structure (floodgate, regulator) was decided based on a problem analysis for Thailand greatest flood in 2011. The RID "Monkey cheek" study revealed that the major problems were from a combination of: i) heavy rainfall from the five Typhoon events in 2011; ii) exceeding capacity of the existing floodgates/regulators in the GCF project area; iii) topographical conditions of rivers (narrow, shallow, bottleneck). Figure 31 shows the relationship of a channel capacity (m^3/s) in the red line against the river discharge of the Ping Yom Nan and Chao Praya Rivers in/and around the project areas. It concludes that there is a recurring flooding area from August – November especially in Yom and Nan Rivers (station Y16, Y17, N7A and N8A)

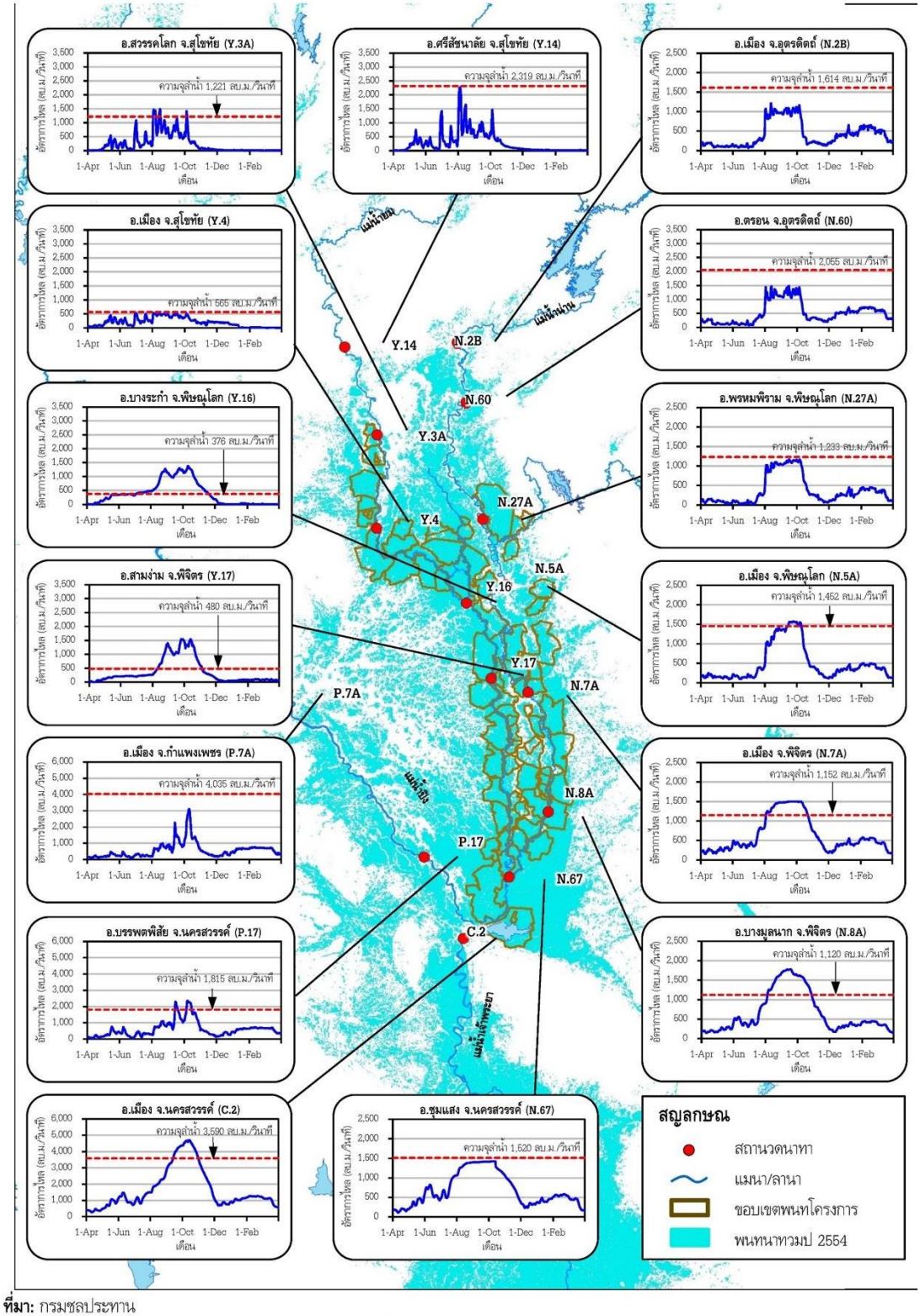

ที่มา: กรมชลประทาน

รูปที่ 4.5.2-1 พื้นที่น้ำท่วมในปี 2554 บริเวณพื้นที่โครงการ

Figure 31: Greatest flood areas in 2011 within the feasibility study of the Monkey Cheek project

The study further shows that upstream areas were at maximum capacity to cope with the high water volume and high flow rates, and the downstream areas (Phisanulok province- Y16, Phichit province –N7A, N8A, Nakhon Sawan province-C2) exceeded their carrying capacities. As a result, the existing irrigation infrastructure (floodgates, regulators and dikes) broke due to excessive flood peaks and water velocities, while the carrying capacity of irrigation structures were exceeded. As a consequence the greatest floodwaters drained into the Chao Praya River starting from Nakhon Sawan province. This area is controlled and managed by several weirs, diversion structures and irrigation canals – with the discharge of the Yom River reducing from 2500m^3/s at the upstream section to 550m^3/s at Sukhothai, and then around 350 m^3/s at the outlet of the project area, predominately due to reduced transport capacity and encroachment of the natural floodplain along the sections. Figure 32 shows river capacity of each river section.

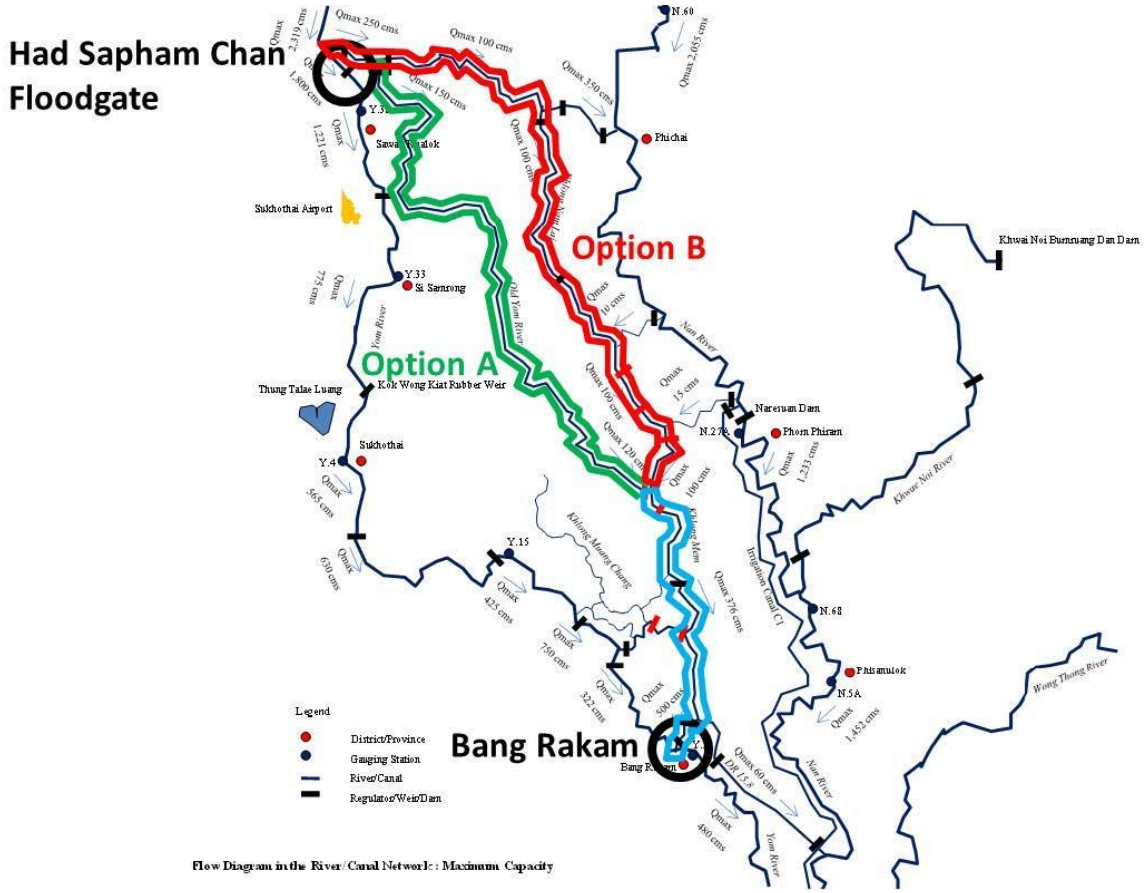

Figure 32: Maximum flow capacities.

A combination of Yom and Nan rivers that is narrow and shallow and the limited capacity of existing infrastructures (floodgates, regulators, embarkment) within the project sites cause flooding within the project areas, therefore the project proposes to increase the capacities of existing infrastructure from 30-120 m^3/s to 50-500 m^3/s, together with EbA measures to further retain waters in upstream areas. As the existing carrying capacity of the infrastructures within Chao Praya River basin is sufficient and the river and its tributaries are wider than the Yom and Nan rivers, discharge normally flow without flooding problems if the Yom and Nan rivers do not flood/exceed their capacities.

The proposed improvements of existing irrigation infrastructures (floodgates, regulators and channels) was based on the aforementioned analysis for the highest flood in 2011. The Feasibility Study and Environmental Impact assessment (EIA) of potential sites for developing the Monkey Cheek areas in lowlands above Nakhon Sawan Province was completed in April 2017. The study covers the GCF project area that was initiated in the same year and Figure 33 shows the GCF project areas within the Monkey Cheek areas.

The Monkey Cheek areas are defined based on detailed study on geology, geography, flood, transportation infrastructure, land use, law, socio-economic profile, wetland, water demand, climate change information, hydrological and hydraulic modelling, public consultation. The total of 69 areas in Suthothai, Phisanulok, Phichit, Nakhon Sawan provinces are defined as a potential area for developing the Monkey Cheek areas, which will serve as temporary detention areas in the irrigation areas north of Nakhon Sawan province and/or natural lowland areas for temporarily controlling floodwaters so as to reduce the peak floods in Yom and Nan Rivers. The engineering and management options must be acceptable to local stakeholders in the areas and the four (4) GCF proposed Monkey Cheek areas are surrounded by existing irrigation structures.

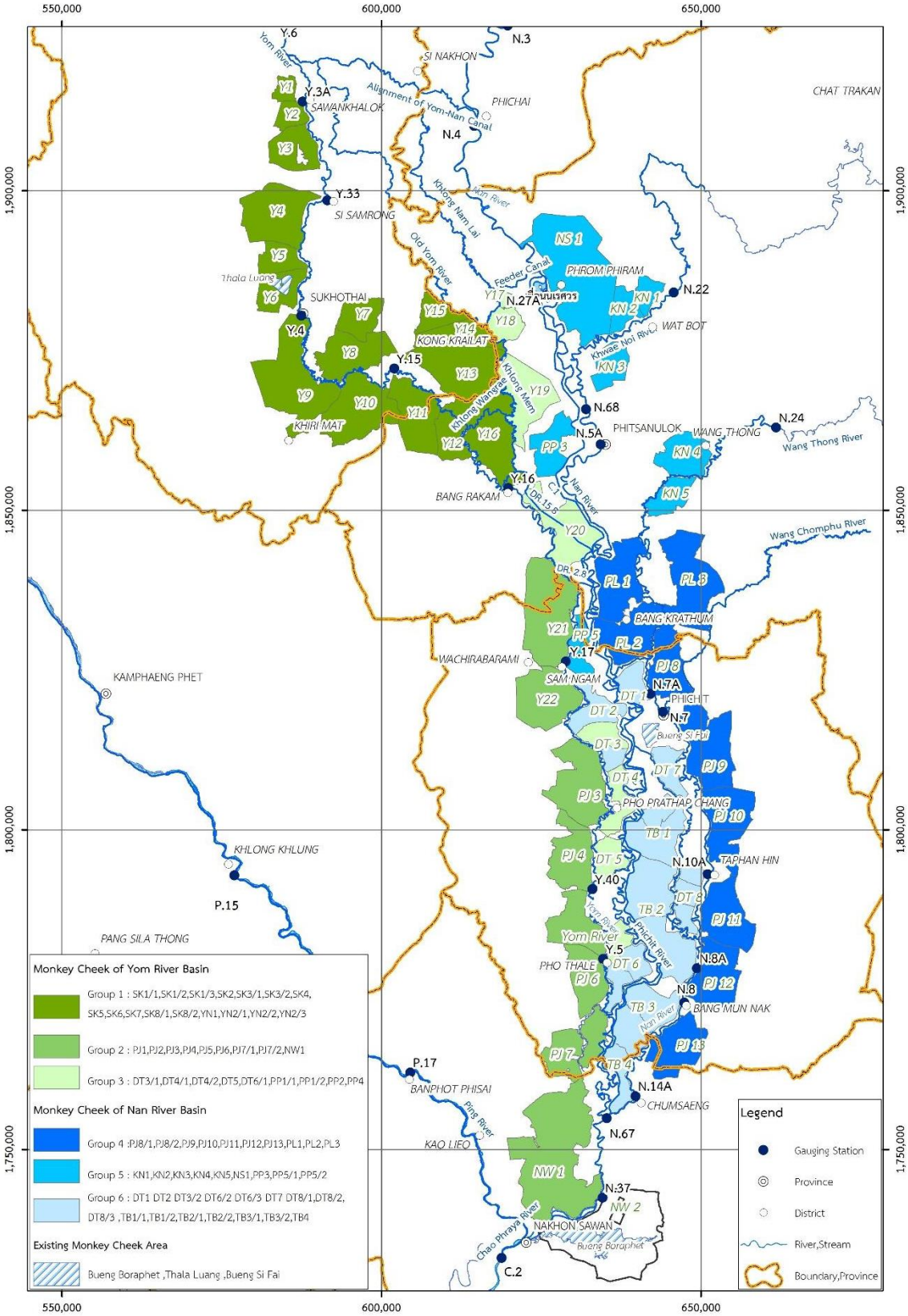

Figure 33: Monkey Cheek areas in Yom and Nan river basins (end at the water metering station in Nakhon Swan province, C.2)

6.2.2 IMPROVED FLOOD MANAGEMENT CAPACITIES

The greatest flood 2011 problem analysis informed RID to improve the efficiency of the irrigation system. The irrigation areas are surrounded by flood dikes, with drain structures and ditches technically suitable for controlling inflows and outflows. However, the existing irrigation components were designed purposely for irrigation water distribution. Consequently, it is necessary to improve these structures and add some components in order to enable inflow-outflow control and management during flood crisis and when the Monkey Cheeks (EbA) need to be used.

The Monkey cheek Feasibility study modelled the water level before and ***after*** the Monkey cheeks are established, based on 3 hydrological and hydraulic models (NAM hydrological model, MIKE Hydraulic River, MIKE Hydraulic Basin). According to the modelling for the Money Cheeks phase 1 (4 Monkey Cheeks within the GCF project area), water flows and levels downstream of the Yom and Nan river basins (discharge to Cha Phraya river basin) are as follows:

Water metering station	2011 (Tr = 45)		2006 (Tr = 20)		2010 (Tr =6)		2007 (Tr = 4)	
	Water level (meter)	Water flow rate (m^3/s)	Water level (meter)	Water flow rate (m^3/s)	Water level (meter)	Water flow rate (m^3/s)	Water level (meter)	Water flow rate (m^3/s)
Y.17, Sam-Ngam district, Phichit province	- 0.018	-15.21	-0.011	-8.32	-0.073	-16.4	+0.035	+8.79
N.7A, Mueang District, Phichit province	-0.18	-1.09	-0.002	-0.75	+0.052	+1.39	+0.019	+4.99
N. 67 Chum- Seang district, Nakhon Sawan	-0.75	-11.34	-0.004	-4.54	+0.047	+39.3	+0.023	+18.66
C.2 Mueang district, Nakhonsawan province	-0.006	-7.73	-0.001	-9.2	+0.01	+6.5	+0.03	+20.50

Remark: (-) reduce (+) increase

The above table shows a water level and water flow rate of each station Y.17, Y.7A, N.67, C2 for a different return period of catchment rainfall; 45-year, 20-year, 6-year, 4-year. The water level and flow rate at the 4 water metering stations for the catchment rainfall return period 45-year and 20-year are reduced whereby they will be increased for catchment rainfall return period 6-year and 4-year. If the Monkey Cheek project implements in the Phisanulok, Suthothai, Uttaradit (GCF project areas), the water level and its flow rate at the water metering stations in downstream areas (Phichit, Nakhonsawan) will be reduced. It concludes that the Monkey Cheeks area in Yom and Nan river basins will be a long term measures for flood and drought mitigation.

7 SUMMARY AND CONCLUSIONS

7.1 HISTORICAL TRENDS IN CLIMATE

Trends at individual stations are difficult to interpret, as they may be affected by systematic and non-systematic errors in the data series, whereas long-term gridded data are conditional on the continuity of station record contributing to the dataset. We have therefore used both datasets to show where they are consistent and trends can be considered robustly independent of the dataset used.

Weak and inconsistent rainfall trends, as present in the Chao Phraya basin, can hardly be interpreted as any systematic drivers behind historical extreme events (be it droughts or floods). Additionally, linking the weak and statistically not-significant rainfall trends present in the Chao Phraya basin to anthropogenic climate change is conceptually difficult, as such trends may arise purely as a random effect of natural climate variability. This is additionally compounded by the presence of multi-decadal variability, with lack of clear long-term trends.

There are, however, relatively strong and consistent historical trends in air temperature, with a stronger signal in mean and minimum temperatures, and weaker in maximum temperature, with consequent implications for drought. As demonstrated, although there is no clear signal in rainfall-based drought indices, a rainfall-evaporation based index (SPEI) shows clearer and consistent signals, with an overall increase in drought, and statistically significant increases in the frequency of SPEI-indexed drought during the last 100 years.

The increase in drought frequency is also conditional on factors such as the quality of the data (it is derived from gridded CRU data, and might be affected by a changing set of stations in that dataset) and the adopted evaporation formula (SPEI is a combination of rainfall and potential evaporation, the latter calculated from air temperature). Whilst different potential evaporation formulas have different sensitivities to temperature, the results are consistent with the strong trends in temperature in gridded and station data. These trends are consistent with global temperature trends and trends in GHG concentrations. This particular trend is therefore expected to increasingly affect local climates in the future.

7.2 Future changes in climate, flood risk, drought and crop water requirements

Climate projections, utilizing multi-model, multi-method and multi-generational ensembles, indicate increases in annual rainfall in the long-term, with signals emerging in the near future. Importantly, while there is a considerable uncertainty about the trajectory of the future climate as manifested by the spread of the multi-model ensembles, it should be noted that there are few projections of a “drier” future, i.e. one characterized by lower than historical annual rainfall. Importantly, all projections indicate increases in rainfall during the main rainfall season.

Projections show that climate change affects the two main variables of hydrological significance - rainfall and air temperature - in a way that the changes may compensate for each other to some extent - i.e there is an increase in rainfall, but also an increase in potential evaporation. Importantly, however, the increases in these two variables follow slightly different trajectories and manifest differently for different seasons. This has implications for drought, with one consequence that future drought risk on annual and longer timescales is expected to reduce in the long-term, once increases in annual rainfall totals exceed increases in potential evapotranspiration. However, as demonstrated through the drought frequency analyses, near future drought will be dominated by increases in evaporation and the frequency of droughts, with increases in rainfall not yet of a magnitude that can compensate for increases in evaporation.

The strong impact of the projected increase in air temperature and PET on agricultural water demand is evident already in the near future, where both crop water demand and irrigation water requirements increase by up to 30% compared to those in the historical period. This means that crops will continue to require more water to meet their physiological needs in the future and that future changes in rainfall are insufficient to meet those needs. This will require either access to more irrigation water, improvements in water use efficiencies, use of less water intensive crops, or climate smart agricultural practices to reduce evaporation and irrigation requirements.

Projected increases in annual total rainfall are largely due to a relatively strong increase in rainfall during the peak of the rainy season (Aug-Oct), which has strong implications for flood risk. The Wichakul et al. 2014 study of hydrological impacts, based on a single projection (climate model) characterized by a relatively weak signal of rainfall change, indicates increases in flood risk in the future. It is clear from that study that the weak rainfall signal is amplified in the hydrological model (and the actual hydrological system) resulting in increases in streamflow in the lower parts of the basin that are manifested throughout the year, but mostly during peak flood conditions. Additionally, the Wikachul et al. 2014 results are more than likely a lower estimate of potential increases in streamflow as the rainfall used in the Wikachul et al. 2014 simulations is at the lower bound of estimated increases from the full suite of GCMs/RCMs analysed here. Although hydrological responses from rainfall increases projected by the broader suite of GCMs/RCMs have not been explicitly modelled, it is clear from the comparison of ensemble rainfall projections with the projected rainfall used by Wikachul et al. 2014, that any such hydrological modelling would simulate significantly higher increases in flood runoff and streamflow in the future.

Such a conclusion is supported by Kotsuki et al., (2014) utilising a range of GCMs and scenarios. That study also shows that increases in streamflow are simulated using all models and scenarios for both near and long term. Importantly, increases in flood streamflow are of a magnitude comparable to the holding capacities of the main dams. It is therefore clear that future changes in climate are expected to result in considerable increases in flood risk in the Chao Phraya river.

The magnitude and spatial distribution of projected increases in streamflow will be conditional on a particular trajectory and spatial distribution of future rainfall, and these, as projected by the suite of GCMs are uncertain. The quantitative determination of future streamflow will inherit that uncertainty, though as argued above the overall qualitative message is unlikely to change; the expectation is for significant increases in streamflow, and consequently increases in flood risk. However, given this quantitative uncertainty, planning and preparation for a particular, narrowly-defined, spatially and temporarily-constrained scenario is not advised as it may result in sub-optimal planning, which neither responds to current flood risks nor those in the future which actually materialise.

REFERENCES

Allen, R. ., Pereira, L. ., Raes, D., & Smith, M. (1991). Crop evapotranspiration - guidelines for computing crop water requirements. *FAO Irrigation and Drainage Paper No.56, FAO*.

Funk, C.C., Peterson, P.J., Landsfeld, M.F., Pedreros, D.H., Verdin, J.P., Rowland, J.D., Romero, B.E., Husak, G.J., Michaelsen, J.C., and Verdin, A.P., 2014, A quasi-global precipitation time series for drought monitoring: U.S. Geological Survey Data Series 832, 4 p., http://dx.doi.org/110.3133/ds832.

Harris, I., Jones, P. D., Osborn, T. J., & Lister, D. H. (2014). Updated high-resolution grids of monthly climatic observations - the CRU TS3.10 Dataset. *International Journal of Climatology*, *34*(3), 623–642. https://doi.org/10.1002/joc.3711

Kotsuki, S., Tanaka, K., & Watanabe, S. (2014). Projected hydrological changes and their consistency under future climate in the Chao Phraya River basin using multi-model and multi-scenario of CMIP5 dataset. *Hydrological Research Letters*, 8(1), 27–32. https://doi.org/10.3178/hrl.8.27

McKee, T. B., Nolan, J., & Kleist, J. (1993). The relationship of drought frequency and duration to time scales. *Preprints, Eighth Conf. on Applied Climatology, Amer. Meteor, Soc.*

Schneider, Udo; Becker, Andreas; Finger, Peter; Meyer-Christoffer, Anja; Ziese, Markus (2018): GPCC Full Data Monthly Product Version 2018 at 0.5°: Monthly Land-Surface Precipitation from Rain-Gauges built on GTS-based and Historical Data. DOI: 10.5676/DWD_GPCC/FD_M_V2018_050

Sen, P. K. (1968). Estimates of the Regression Coefficient Based on Kendall's Tau. *Journal of the American Statistical Association*, *63*(324), 1379–1389. https://doi.org/10.1080/01621459.1968.10480934

Trakuldit T, Faysse N. Difficult encounters around "monkey cheeks": Farmers' interests and the design of flood retention areas in Thailand. J Flood Risk Management . 2019;12 (Suppl. 2):e12543

Vicente-Serrano, S. M., Beguería, S., & López-Moreno, J. I. (2010). A multiscalar drought index sensitive to global warming: The standardized precipitation evapotranspiration index. *Journal of Climate*, *23*(7), 1696–1718. https://doi.org/10.1175/2009JCLI2909.1

Wichakul, S., Tachikawa, Y., Shiiba, M., Yorozu, K., 2013a. Developing a regional distributed hydrological model for water resources assessment and it application to the Chao Phraya River Basin. J. Japan Society of Civil Eng. B1 (Hydraulic Eng.). 69(4), 43–48.

Wichakul, S., Tachikawa, Y., Shiiba, M., Yorozu, K., 2013b. Development of a flow routing model including inundation effect for the extreme flood in the Chao Phraya River Basin, Thailand 2011. J. Disaster Research. 8(3), 415–423.

Wichakul, S., Tachikawa, Y., Shiiba, M., Yorozu, K., 2014. Prediction of water resources in the Chao Phraya River Basin, Thailand. Proceeding from Hydrology in Hydrology in a Changing World: Environmental and Human Dimensions, 7th Global FRIEND-Water Conference (IAHS). Publ. 363. Montpellier, France. (in press)

Wichakul, S., Tachikawa, Y., Shiiba, M., Yorozu, K., 2015. River discharge assessment under a changing climate in the Chao Phraya River, Thailand by using MRI-AGCM3.2S. J. Hydrological Research Letter. 9 (4), 84-89.